

1 **Supplemental Information for:**  
2 **Secondary Organic Aerosols from Anthropogenic Volatile Organic Compounds Contribute**  
3 **Substantially to Air Pollution Mortality**

4

5 Benjamin A. Nault et al.

6

7 Correspondence: Benjamin A. Nault (bnault@aerodyne.com), Jose L. Jimenez  
8 (jose.jimenez@colorado.edu)

## 9 S1 Emission Inventories for Various Urban Areas around the World

10 All BTEX (benzene, toluene, ethylbenzene, and xylenes) and non-BTEX aromatic  
11 emissions are shown in Table S5 (BTEX) or Table S8 (non-BTEX aromatics). The emission  
12 ratios are derived from ambient measurements utilizing photochemical aging techniques (Nault  
13 et al., 2018).

14 Details of the emission inventories for cities in the US, for Beijing, and for London/UK  
15 used here to estimate the IVOC:BTEX emission ratio (Fig. 5) and thus the IVOC emissions can  
16 be found below. Briefly, emissions for the US are based on McDonald et al. (2018), for China on  
17 the Multi-resolution Emission Inventory for China (MEIC) (Zhang et al., 2009; Zheng et al.,  
18 2014, 2018; Liu et al., 2015; Li et al., 2017, 2019), and for the UK on the National Atmospheric  
19 Emissions Inventory (NAEI) (EMEP/EEA, 2016). The IVOC:BTEX emission ratio from  
20 inventories are multiplied with the observed BTEX, either reported value from studies (NE US  
21 aircraft (Warneke et al., 2007), Los Angeles (de Gouw et al., 2017), Beijing (Wang et al., 2014),  
22 and New York City (Warneke et al., 2007)) or estimated from Eq. 3 (London), to estimate IVOCs  
23 emitted in each region (Table S5). This ensures IVOC emissions used in our calculations  
24 properly reflect differences in mixtures of emission sources (e.g., mobile sources versus VCPs)  
25 that vary by continent for each field campaign. Additionally, we rely on inventories for  
26 estimating atmospheric abundances of IVOCs because it has been challenging to measure the full  
27 range of IVOC precursors that are emitted into urban air due to many of the IVOCs from VCPs  
28 being oxygenated VOCs. These compounds are challenging to measure using traditional  
29 instrumentation (e.g., gas chromatography-mass spectrometry), leading to potential  
30 underestimation of the IVOC emission ratios (Zhao et al., 2014, 2017; Lu et al., 2018). The

31 bottom-up IVOC:BTEX ratios for the US, Beijing, and UK are described in greater detail below.  
32 IVOC emissions are classified based on their vapor pressure (effective saturation concentration:  
33  $10^3 < C^* < 10^6 \mu\text{g m}^{-3}$ ), with the vapor pressure estimated by the SIMPOL.1 model (Pankow and  
34 Asher, 2008). The ASOA yields and rate constants for IVOC oxidation were parameterized with  
35 data from n-tridecane and n-pentadecane for gasoline and diesel emissions, respectively (Jathar  
36 et al., 2014), and for VCPs, the yields and rate constants for IVOC oxidation were parameterized  
37 with data from n-tetradecane (McDonald et al., 2018).

38         Similar to IVOCs, the ability to measure the full range of SVOCs emitted into urban air is  
39 challenging. Therefore, we estimate SVOC emission ratios relative to POA mass concentrations  
40 (Table S9), as described by Ma et al. (2017). For the hydrocarbon-like portion, we used the  
41 volatility distribution from Worton et al. (2014) to estimate SVOC, as this is associated with  
42 fossil fuel emissions from transportation (Zhang et al., 2005). For the other POA, we used the  
43 volatility distribution from Robinson et al. (2007), as this POA is typically cooking primary  
44 aerosol. These profiles were selected to be consistent with Ma et al. (2017).

45         To estimate the SVOC mass concentration in equilibrium with POA (Table S9), in each  
46 bin (e.g.,  $C^* = 0, 1, 2$ ), the normalized POA mass concentration is first multiplied by the fraction  
47 of POA measured in each bin from literature. For other POA, which includes biomass burning  
48 and cooking OA, the fraction of POA found in  $\log_{10}C^* = 0, 1$ , and  $2$  are  $0.22, 0.34$ , and  $0.44$ ,  
49 respectively (Robinson et al., 2007), and for vehicular POA, the fraction of POA found in  
50  $\log_{10}C^* = 0, 1$ , and  $2$  are  $0.42, 0.40$ , and  $0.18$ , respectively (Worton et al., 2014). So, for example,  
51 for NE US, this would correspond to normalized POA mass concentrations (POA/ $\Delta\text{CO}$ ) of  $5.1$ ,  
52  $4.9$ , and  $2.2 \mu\text{g sm}^{-3} \text{ ppmv}^{-1}$  for  $\log_{10}C^* = 0, 1$ , and  $2$ , respectively. Then the total POA + SVOC

53 normalized mass concentration for that bin is obtained by dividing the amount of material found  
54 in the particle-phase for that bin at the average temperature ( $\sim 298$  K) and OA mass concentration  
55 ( $\sim 10 \mu\text{g sm}^{-3}$ ). So, taking NE US as an example, for  $\log_{10}C^* = 0, 1, \text{ and } 2$ , 9%, 50%, and 91% of  
56 the material, respectively, will be in the gas-phase versus the aerosol-phase, leading to the  
57 normalized mass concentration of SVOC as inputs into the model of 0.39, 3.8, and  $17.1 \mu\text{g sm}^{-3}$   
58  $\text{ppmv}^{-1}$ . The values of 9%, 50%, and 91% were used for NE US, Los Angeles, London, and  
59 Beijing, as the ambient temperatures were  $\sim 298$  K. For New York City, as the study took place  
60 during winter, values of 3%, 22%, and 74% were used as the ambient temperature was  $\sim 273$  K.

61 Fig. S6 shows the calculated emission ratio versus saturation concentration ( $c^*$ ) for the  
62 cities with emission inventories. The saturation concentration for SVOC was determined as part  
63 of the estimation procedure discussed above. For IVOC, the emission ratios for the different  
64 sources (gasoline, diesel, other fossil fuel sources, and VCP emissions) were split into the  
65 volatility bins, as in McDonald et al. (2018). Finally, for BTEX and non-BTEX aromatics, and  
66 other VOC emission ratios (see Fig. S6 for references for the other VOC emission ratios), CRC  
67 (Rumble, 2019) or SIMPOL.1 (Pankow and Asher, 2008) (for estimating vapor pressures not in  
68 CRC) was used to estimate the saturation concentrations.

69

## 70 **S1.1 US Emission Inventories**

### 71 *Anthropogenic VOC emissions*

72 The US emissions of VOCs is based on a mass balance estimate of the petrochemical  
73 industry reported by McDonald et al. (2018). Briefly, fuel sales and chemical product use are  
74 estimated from publicly available reports on energy use, chemical production, economic surveys,

75 and freight shipments. Mobile source emission factors are from prior work quantifying both  
76 on-road and off-road engines (McDonald et al., 2013, 2015). Evaporative sources of  
77 transportation fuels are considered in addition to tailpipe exhaust (Pierson et al., 1999). VCP  
78 emission factors are based on literature values, including from the indoor environment, and  
79 reported in McDonald et al. (2018). Other fossil energy sources of VOCs, such as from oil  
80 refineries and industry, are taken from official inventories reported by the California Air  
81 Resources Board (CARB, 2013) or US Environmental Protection Agency (NEI, 2015).  
82 McDonald et al. (2018) reported fossil-VOC emissions for the Los Angeles basin in the year  
83 2010.

84

#### 85 *Speciation of VOC emissions*

86 The total VOC emissions are speciated to estimate BTEX and IVOC emissions from  
87 petrochemical VOC sources. Briefly, gasoline and diesel exhaust, gasoline fuel, and headspace  
88 vapors are based on profiles reported in the literature from the Caldecott Tunnel (Gentner et al.,  
89 2012, 2013). Speciation profiles of VCPs are based on California Air Resources Board surveys  
90 of architectural coatings (Davis, 2007) and consumer products (CCPR, 2015). Other industrial  
91 solvent uses and point/area source emissions are from the EPA SPECIATE (v4.4) database (EPA,  
92 2014).

93

#### 94 *Extrapolating IVOC/BTEX ratios from 2010 Los Angeles to other field campaigns*

95 In the ASOA mass closure estimation, three separate field campaigns are utilized from  
96 the US: NEAQS 2002 (Boston/New York City), CalNex 2010 (Los Angeles), and WINTER

97 2015 (New York City outflow). These field campaigns span two megacities (Los Angeles and  
98 New York City), ~one decade, and two seasons (summer versus winter). Here, we discuss how  
99 each of these variables could affect the IVOC/BTEX emissions ratio. We focus the discussion on  
100 mobile sources and VCPs because these are the dominant contributors to BTEX and IVOCs.

101       The IVOC/BTEX emissions ratio could be affected by the population density of a city. It  
102 is well-established that per capita transportation fuel use decreases with increasing population  
103 density (Gately et al., 2015), whereas VCP usage is expected to scale with population. Relative  
104 to Los Angeles, the per capita fuel use in New York City is ~2 times lower (Gately et al., 2015),  
105 resulting in lower on-road transportation VOC emissions relative to VCPs. Because aromatics  
106 are mainly found in gasoline, whereas the IVOCs have a higher contribution from VCPs, the  
107 IVOC/BTEX ratio is expected to be higher in New York City than Los Angeles.

108       To assess impacts of annual trends on the IVOC/BTEX ratio, we utilize long-term trend  
109 analyses of mobile source VOC emissions in Los Angeles (McDonald et al., 2013, 2015; Hassler  
110 et al., 2016). The main effect is that on-road gasoline emissions have decreased with time, both  
111 from the tailpipe of vehicles (McDonald et al., 2013) and of gasoline-related VOCs in ambient  
112 air measurements (Warneke et al., 2012). We utilize the EPA Trends Report to scale VOC  
113 emissions for other anthropogenic sectors, including VCPs and industrial sources  
114 (<https://www.epa.gov/air-emissions-inventories/air-pollutant-emissions-trends-data>). The EPA  
115 Trends Report suggests that VCP (or solvent) emissions decreased by ~30% between 2002 and  
116 2010, including efforts to reduce the VOC content of architectural coatings (Matheson, 2002).  
117 After 2010, the emissions have been slightly increasing, likely due to population growth.

118 Because both mobile sources and VCP emissions are decreasing with time, the IVOC/BTEX  
119 emissions ratio is not significantly altered.

120 Lastly, the effects of seasonality influence on-road transportation emissions through: (i)  
121 increased VOC emissions in winter relative to summer from cold-starting engines, and (ii) lower  
122 evaporative emissions due to colder ambient temperatures. We estimate that exhaust emissions  
123 from passenger vehicles increases by ~50% due to higher cold-start emissions in winter relative  
124 to summer based on the EPA MOVES model (MOVES, 2015). Evaporated gasoline and  
125 headspace vapors are known to exhibit a temperature-dependence (Rubin et al., 2006), and  
126 estimated to be ~20% and ~80% lower, respectively, based on typical wintertime temperatures of  
127 New York City relative to summertime Los Angeles. Due to compensating factors between  
128 cold-start engines and evaporated fuels, the IVOC/BTEX emissions are not significantly affected  
129 by seasonality.

130 Overall, when taking into account differences in population density between Los Angeles  
131 and New York City, trends of mobile source and VCP emissions over time, and seasonality, the  
132 IVOC/BTEX emission ratios range between ~2.3 to 2.7, which is a relatively small range. This  
133 sensitivity analysis helps explain why the enhancement observed in SOA scales with BTEX  
134 levels in the urban atmosphere.

135

## 136 **S1.2 Beijing Emission Inventory**

### 137 *Anthropogenic VOC emissions*

138 The total VOC emissions of Beijing were developed following the bottom-up framework  
139 of the Multi-resolution Emission Inventory for China (MEIC) model (available at

140 <http://www.meicmodel.org>), based on a technology-based methodology. The details of activity  
141 rates, emission factors, technology distribution, and control measures configured in the MEIC  
142 model are summarized in a series of papers (Zhang et al., 2009; Zheng et al., 2014, 2018; Liu et  
143 al., 2015; Li et al., 2017, 2019).

144 In the MEIC model, a detailed four-level source classification system, representing  
145 sector, fuel/product, technology/solvent type, and end-of-pipe pollutant abatement facilities, was  
146 established by including over 700 emitting sources for each province. All anthropogenic sources,  
147 including power plants, industrial sources, volatile chemical products, fossil fuel burning in  
148 residential stoves, transportation were all considered.

149 Power plants are treated as point sources in the MEIC model. The VOC emissions were  
150 derived from the China coal-fired Power Plant Emissions Database (CPED, (Liu et al., 2015)),  
151 which is developed based on information of each unit on fuel type, fuel quality, combustion  
152 technology, etc.

153 Volatile chemical products are comprised of solvent use applied for architecture, vehicles,  
154 wood, and other industrial purposes, glue use, printing, pesticide use, and domestic solvent use.  
155 The market share of waterborne and solvent-based paint is further taken into account for each  
156 source category. For the on-road transportation sector, the improved emissions developed by  
157 Zheng et al. (2014) were integrated into the framework of MEIC, which estimated the vehicle  
158 population and emission factors at a county level. Both the VOC emissions in running mode and  
159 evaporation were considered. Emission standards covering pre-Euro I and Euro I to Euro V in  
160 Beijing were applied for each vehicle type (Zheng et al., 2018; Li et al., 2019). Regarding  
161 oxygenated volatile organic compounds (OVOCs), the emission factors for on-road vehicles



162 were corrected, as current emission factors are only for non-methane hydrocarbons (NMHC).  
163 Correction ratios of 1.32, 1.08, 1.10, and 1.06 were applied for heavy-duty and light-duty diesel  
164 vehicles, and heavy-duty and light-duty gasoline vehicles, respectively, to the original values to  
165 comply with the follow-up speciation for the total VOC, following the method of Li et al. (2014,  
166 2019).

167

#### 168 *Speciation of VOC emissions*

169 Emissions by individual chemical species were developed based on the  
170 profile-assignment approach (Li et al., 2014, 2019). First, a “composite” profile database for  
171 China was established by integrating the local profiles and supplementing it with the SPECIATE  
172 v4.5 database for absent sources ((Simon et al., 2010), available at:  
173 <https://www.epa.gov/air-emissions-modeling/speciate-version-45-through-40>). The detailed  
174 procedure for developing the composite profile database is illustrated in Li et al. (2014). In brief,  
175 for sources where there are significant differences in technology or legislation between China  
176 and western countries, only local profiles are used; otherwise, all candidate profiles are included  
177 for further compilation in the composite profile database. Local profiles covering most of the  
178 important sources were gathered and reviewed, including biofuel combustion, coal combustion,  
179 asphalt production, oil production, refinery, paint use, gasoline evaporation, gasoline vehicle  
180 exhaust, diesel vehicles, and so on, as detailed illustrated in Li et al. (2019).

181 Then, profiles for all combustion-related sources, including fossil fuel combustion in  
182 power plants, industry, residential, and transportation sectors were reviewed, and incomplete  
183 profiles that were absent from the OVOC fractions were corrected by appending the component

184 of “OVOC” with fractions derived from the “complete” profiles for the same source. After  
185 OVOC correction, all “candidate” profiles were averaged by species to establish the composite  
186 profile database. Finally, the composite profile to each source was assigned by setting up the  
187 source linkage between the profile database and the inventory. Emissions by individual chemical  
188 species for each source were then further developed.

189

### 190 **S1.3 London/United Kingdom Emission Inventory**

#### 191 *Anthropogenic VOC emissions*

192 The National Atmospheric Emissions Inventory (NAEI) estimates UK emissions of  
193 VOCs from anthropogenic sources following methods in the EMEP/EEA Emissions Inventory  
194 Guidebook (EMEP/EEA, 2016) for submission under the revised EU Directive 2016/2284/EU on  
195 National Emissions Ceilings (NECD), available at:  
196 <https://eur-lex.europa.eu/legal-content/EN/TXT/PDF/?uri=CELEX:32016L2284&from=EN>, and  
197 the United Nations Economic Commission for Europe (UNECE) Convention on Long-Range  
198 Transboundary Air Pollution (CLRTAP), available at:  
199 [http://www.ceip.at/ms/ceip\\_home1/ceip\\_home/reporting\\_instructions/reporting\\_programme/](http://www.ceip.at/ms/ceip_home1/ceip_home/reporting_instructions/reporting_programme/).

200 The NECD and CLRTAP define those VOC sources to be included and excluded from the  
201 national inventory (for example, emissions of NMVOCs from biogenic sources are not included).  
202 The Guidebook provides estimation methodologies and default emission factors for each source  
203 category, although countries can use country-specific emission factors where these are deemed  
204 relevant. The NAEI currently covers organic emissions from around 400 individual source  
205 categories, with a large contribution from a diverse range of industrial processes and solvents,

206 but with very few individually dominant sources. The inventory then speciates emissions into  
207 ~650 individual compounds, or groups of compounds. Groupings of organics, for example,  
208 expressed as ‘sum of all C14 compounds,’ make up a substantial fraction of IVOC emissions,  
209 rather than being reported as individual compounds.

210 Emissions from the use of solvents and other volatile chemicals in industry and in  
211 consumer products, fuel production and distribution, food and drink manufacture and other  
212 non-combustion industrial processes accounted for 72% of all UK NMVOC emissions in 2017,  
213 according to the NAEI. Both the solvent and industrial process sectors cover a diverse range of  
214 emission source categories: the NAEI identifies 136 separate categories across the two sectors

215 For the road transport sector, the NAEI reports exhaust emissions of NMVOCs and its  
216 emissions from evaporative losses of fuel vapor from petrol vehicles. Emissions from re-fueling  
217 at filling stations are reported separately under the fugitive emissions from the fuel distribution  
218 sector. The method used for road transport in the NAEI follows the method in the European  
219 COPERT 5 model and described in the EMEP/EEA Emissions Inventory Guidebook. The  
220 method uses average speed-related emission factors for hot exhaust emissions of total  
221 hydrocarbons for detailed vehicle categories (vehicle type, weight and/or engine size) and Euro  
222 standards for petrol cars, diesel cars, petrol and diesel light goods vehicles, rigid and articulated  
223 HGVs, buses and coaches, and mopeds and motorcycles, and combines these with detailed traffic  
224 and fleet activity data derived from information provided by DfT. Separate estimates are made of  
225 methane emissions for each vehicle type and subtracted from the THC emissions to derive the  
226 NMVOC emissions.

227        Evaporative emissions from vehicles are estimated in the NAEI, using the Guidebook  
228 method for three different processes: diurnal losses, hot soak, and running losses. Emissions are  
229 dependent on ambient temperature and fuel vapor pressure and different factors are provided for  
230 vehicles with and without carbon canisters for evaporative emission controls. All vehicles from  
231 Euro 1 onwards are fitted with these devices; so, evaporative emission have been decreasing  
232 from the early 1990s with the penetration of these vehicles in the fleet. The method also takes  
233 into account the reduction in Reid Vapour Petrol of petrol sold in the UK since 2000, as required  
234 for compliance with the EU Fuel Quality Directive 98/70/EC, amended by Directive  
235 2009/30/EC.

236

#### 237        *Speciation of VOC emissions*

238        The NAEI is considered to adequately reflect annual real world emissions of BTEX (see,  
239 for example, eddy covariance flux comparisons in London by Langford et al. (2010) and Vaughn  
240 et al. (2017)); so, those values are taken directly from the NAEI and used here. IVOCs, and  
241 particularly long chain hydrocarbons, are included in many cases in the inventory as groups, but  
242 their emissions are known to be significantly underestimated when compared against field  
243 observations. We use the observations of Dunmore et al. (2015), made in wintertime central  
244 London in 2012, as guide to uprate NAEI emissions for IVOC species based on the estimated  
245 discrepancies between inventory and field observation reported for each carbon number above  
246 C10. This leads to some significant multipliers being applied to the inventory values, sometimes  
247 of the order 60 to 70. We assume that the same multipliers apply to all sources, since field data

248 does not provide any means to attribute different factors to road transport IVOCs compared with  
249 IVOCs from VCP sources.

250 Since the NAEI represents a reporting of emissions for the purposes of compliance with  
251 international treaties, some fraction of those emissions are not released on the mainland UK. For  
252 this paper, offshore BTEX and IVOC emissions, arising for example from offshore oil and gas  
253 activity, aircraft in cruise, or shipping and emissions associated with overseas Crown  
254 Dependencies are removed from the UK total, since they play no part in determining the  
255 chemical environment of London. The annual NAEI totals are then divided equally to give a  
256 daily national emission.

257

## 258 **S2 ASOA Budget Analysis of Ambient Observations**

259 To calculate the ASOA budget, we used the observed BTEX (Table S5) and non-BTEX  
260 aromatic (Table S8) emission ratios, the emission inventories for IVOC (see above), and  
261 estimated SVOCs from the primary OA emissions (see above). The methods to calculate ASOA  
262 from emissions have been described in detail elsewhere (Hayes et al., 2015; Ma et al., 2017;  
263 Schroder et al., 2018), and are briefly described here. All calculations described were conducted  
264 with the KinSim v4.02 chemical kinetics simulator (Peng and Jimenez, 2019) within Igor Pro 7  
265 (Lake Oswego, Oregon), and are summarized in Fig. S7. A typical average particle diameter for  
266 urban environments of ~200 nm (Seinfeld and Pandis, 2006) is used to estimate the  
267 condensational sink term for the partitioning of gas-to-particle, although condensation is always  
268 fast compared to the experiment timescales. Further, we assume an average 250 g mol<sup>-1</sup> molar  
269 mass for OA and an average SOA density of 1.4 g cm<sup>-3</sup> (Vaden et al., 2011; Kuwata et al., 2012).

270 Finally, all models are initialized with the campaign specific OA background (typically  $\sim 2 \mu\text{g}$   
271  $\text{sm}^{-3}$ ) and POA (Table S9) for partitioning of gases to the particle phase, and ran at the average  
272 temperature for the campaign.

273 For the modeled VOCs (BTEX and non-BTEX aromatics), each species undergoes  
274 temperature-dependent OH oxidation (Table S12), forming four SVOCs that partition between  
275 gas- and particle-phase, using updated SOA yields that account for wall loss (Ma et al., 2017).  
276 For IVOCs, the emission weighted SOA yields and rate constants from the “Zhao” option (Zhao  
277 et al., 2014) of Ma et al. (2017) are used, and the products are apportioned into three SVOC bins  
278 and one low-volatility organic compound (LVOC) bin (Fig. S7). Finally, SVOCs undergo  
279 photooxidation at a rate of  $4 \times 10^{-11} \text{ cm}^3 \text{ molecules}^{-1} \text{ s}^{-1}$  (Dzepina et al., 2009; Hodzic et al., 2010;  
280 Tsimpidi et al., 2010; Hodzic and Jimenez, 2011; Hayes et al., 2015; Ma et al., 2017; Schroder et  
281 al., 2018), producing one product per oxidation step, with yields from Robinson et al. (2007) for  
282 cooking and other SVOCs and yields from Worton et al. (2014) for fossil fuel related SVOCs, as  
283 recommended by Ma et al. (2017). The products from SVOC and IVOC oxidation are allowed to  
284 further oxidize, as highlighted in Fig. S7 and described in prior studies (Hayes et al., 2015; Ma et  
285 al., 2017; Schroder et al., 2018). Generally, each product reacts at a rate of  $4 \times 10^{-11} \text{ cm}^3$   
286  $\text{molecules}^{-1} \text{ s}^{-1}$  to produce some product at one volatility bin lower, adding one oxygen to the  
287 compound for each oxidation (Dzepina et al., 2009; Tsimpidi et al., 2010; Hodzic and Jimenez,  
288 2011; Hayes et al., 2015; Ma et al., 2017; Schroder et al., 2018). An update includes  
289 fragmentation for a fraction of the molecules that are oxidized, as described in Schroder et al.  
290 (2018) and Koo et al. (2014). As shown in Fig. S7, fragmentation of the compound occurs as it is  
291 oxidized and goes down one volatility bin. For further oxidation of SVOCs from the oxidation of

primary IVOCs, one oxygen is added and 0.25 carbon is removed per step, leading to an increase in mass of 1.03 (instead of 1.07) per oxidation step (Koo et al., 2014; Schroder et al., 2018). For further oxidation of products from primary SVOC emissions, one oxygen is added and 0.5 carbon is removed per step, leading to a decrease in mass of 1% (instead of 1.07) per oxidation step (Koo et al., 2014; Schroder et al., 2018).

### **S3 GEOS-Chem Modeling**

The model used in this study is GEOS-Chem v12.0.0 (Bey et al., 2001; The International GEOS-Chem User Community, 2018). This model is used for the following calculations: (1) ASOA apportionment (Fig. 1), (2) apportionment of ASOA to total PM<sub>2.5</sub> for premature mortality calculations (Sect. 5), and (3) sensitivity analysis for ASOA production and emissions on premature mortality calculations. GEOS-Chem is operated at 2°×2.5° horizontal resolution. Goddard Earth Observing System – Forward Processing (GEOS-FP) assimilated data from the NASA Global Modeling and Assimilation Office (GMAO) were used for input meteorological fields. The model was run for 2013 to 2018 to take into account interannual variability of meteorological impacts onto PM<sub>2.5</sub> (therefore, averaging PM<sub>2.5</sub> over variations in meteorology). However, the HTAPv2 emission inventory, which was used for anthropogenic emissions (Janssens-Maenhout et al., 2015), was kept constant for the 5 years. Analysis of the HTAP emissions, compared to other emission inventories, generally showed the highest correlation with observations ( $R^2 = 0.54$ ), versus the other inventories (CEDS  $R^2 = 0.26$ , MACCity  $R^2 = 0.00$ , and RETROv2  $R^2 = 0.04$ ), leading to the selection of this emission inventory. GEOS-Chem simulates gas and aerosol chemistry with ~700 chemical reactions. GEOS-Chem calculates the following

314 PM<sub>2.5</sub> species: sulfate, ammonium, nitrate (Park et al., 2006); black carbon and POA (Park et al.,  
315 2005); SOA (Pye and Seinfeld, 2010; Marais et al., 2016); sea salt (accumulation mode only  
316 (Jaeglé et al., 2011)); and, dust (Duncan Fairlie et al., 2007).

317

### 318 **S3.1 Biogenic SOA**

319 For monoterpene and sesquiterpene SOAs, we used the default complex SOA scheme  
320 (without semi-volatile POA) using the two-product model framework (Pye and Seinfeld, 2010).  
321 This scheme calculates initial oxidation of VOCs with OH, O<sub>3</sub>, and NO<sub>3</sub>, and resulting products  
322 are assigned to four different gas-phase semi-volatile species (TSOA0–3) based on volatilities  
323 ( $c^* = 0.1, 1, 10, 100 \mu\text{g m}^{-3}$ ). Aerosol and gas species fractions are calculated online using the  
324 partitioning theory, and all are removed by dry and wet deposition processes.

325 For isoprene SOA, we used the explicit isoprene chemistry developed by Marais et al.  
326 (2016). All the isoprene-derived gas-phase products, including isoprene peroxy radical,  
327 ISOPOOH, IEPOX, glyoxal, and methylglyoxal, are explicitly simulated. Irreversible  
328 heterogeneous uptake of precursors to aqueous aerosols are further calculated using online  
329 aerosol pH and surface area.

330 GEOS-Chem was used to estimate the relative fractions of the measured SOA in our  
331 studies between anthropogenic and biogenic (isoprene and monoterpene) sources (Fig. 1).  
332 Extensive research has been conducted to evaluate and improve the models performance in  
333 predicting BSOA, as summarized in Table S3. Though these evaluations mainly occurred in the  
334 southeast US, a recent study has also included more global observations to compare with  
335 GEOS-Chem (Pai et al., 2020). Generally, GEOS-Chem appears to overestimate biogenically



336 derived SOA; however, the model predicted SOA is typically within the uncertainty of the AMS  
337 (Table S3). The overestimation, though, would suggest that the fraction of urban SOA may be  
338 under-predicted by this method, whereas the BSOA may be over-predicted. Therefore, in urban  
339 regions, the amount of SOA from biogenic sources may be lower, especially after the rapid SOA  
340 enhancements (within 12 to 24 equivalent photochemical hours that have been observed around  
341 the world (Nault et al., 2018)). Typically the BSOA is present as a regional background and  
342 subtracted for the analyses used in this work, which focus on strong urban plumes on top of that  
343 background (Hayes et al., 2013, 2015).

344

### 345 **S3.2 Default GEOS-Chem Sensitivity to ASOA Simulations**

346 For the sensitivity calculation using the "traditional" ASOA precursors, we used the  
347 two-product model framework (Pye and Seinfeld, 2010). Benzene, toluene, and xylene are  
348 oxidized with OH and converted to peroxy radicals. These peroxy radicals react with HO<sub>2</sub> or NO,  
349 resulting in non-volatile ASOA (HO<sub>2</sub> pathway, ASOAN species in GEOS-Chem) or  
350 semi-volatile ASOA tracers (NO pathway, ASOA1-3 in GEOS-Chem). As is the case for  
351 monoterpene and sesquiterpene SOA above, GEOS-Chem calculates online partitioning and  
352 dry/wet deposition processes for semi-volatile ASOA tracers. Other conditions including  
353 mortality calculation are kept the same as the base simulation above.

354

### 355 **S4 Ozone Sensitivity to ASOA Simulations**

356 A potential issue in the attribution of premature mortality to AOSA is that reducing  
357 emissions that lead to ASOA is that this may impact ozone concentrations. A sensitivity analysis

was conducted, where the ASOA emissions were reduced by 20% (Fig. S14). In general, there is a less than 1% reduction in total ozone concentration in the boundary layer. This is due to the fact that the most important AVOCs that contribute to ozone formation are light alkenes (e.g., ethylene and propylene, Fig. 2), which are not ASOA precursors. Though the reaction rate constant of the ASOA precursors is generally high (Table S12), the concentration of the precursors is low and they thus account for a low percentage of the total ozone production potential (Table S5 through Table S9). For example, the measured OH reactivity (Sect. 3) for two different urban regions was between 15 to 25 s<sup>-1</sup> (Griffith et al., 2016; Whalley et al., 2016) while the OH reactivity for the ASOA precursors for the same region was between 2 to 4 s<sup>-1</sup>. The small contribution to the OH reactivity is in line to the minimal impact to the ozone concentration observed in Fig. S14.

## **S5 Error Analysis of Observations**

The errors that will be discussed here are in reference to Fig. 2 and Fig. 4 and Table S4 either come from the 1 $\sigma$  uncertainty in the slopes (the SOA versus O<sub>x</sub>, HCHO, or PAN values) or propagation of uncertainty in observations. For SOA, we estimate the 1 $\sigma$  uncertainty of ~15%, which is lower than the typical 1 $\sigma$  uncertainty of the AMS (Bahreini et al., 2009) due to the careful calibrations and excellent intercomparisons in the various campaigns (see Table 1 for references for the AMS comparisons). For  $\Delta$ CO, the largest uncertainty is associated with the CO background (Hayes et al., 2013; Nault et al., 2018), and is estimated to be ~10% at 0.5 photochemical equivalent days (Hayes et al., 2013). The uncertainty in the emission ratios is ~10% (Wang et al., 2014; de Gouw et al., 2017); though, it may be higher for the values

380 calculated here due to the uncertainty in CO background, rate constants, and photochemical age.  
381 Therefore, for Fig. 2a, the uncertainty in the y-values is 18% and the uncertainty in the x-values  
382 is 10%. For Fig. 4, the uncertainty in the measurement is 21%.

383 Another potential source of uncertainty may stem from the fit of the data in Fig. 2a, as the  
384 data point from Seoul (KORUS-AQ) could be impacting the fit due to the difference in its value  
385 compared to the other locations. Statistical analysis for the influence of the data from Seoul on  
386 the figure was conducted, including a T-test, Cook's Distance test, and Difference in Fits test  
387 (Table S11). All three statistical tests show that the data from Seoul (and all the data in general)  
388 is not overly influencing the reported slope.

389 A further potential source of uncertainty in this analysis is the calculated VOC emission  
390 ratios for the studies that did not have ratios published previously (Houston 2000, London,  
391 Houston 2013, and Seoul). To investigate how well Eq. 3 does in estimating the VOC emission  
392 ratios, a comparison of the estimated VOC emission ratios versus previously published ratios for  
393 two different cities, Mexico City (Apel et al., 2010; Bon et al., 2011) and Los Angeles (de Gouw  
394 et al., 2017) was made (Table S10). Also, for Mexico City, two locations, an urban and a  
395 suburban site, were compared both against each other (Apel et al., 2010; Bon et al., 2011) and  
396 the calculated values from Eq. 3.

397 First, as shown in Table S10, even for the same location (suburban Mexico City),  
398 different values in the emission ratio, especially for the alkanes, can be observed, by as much as  
399 a factor of 7. This can be partially explained by differences in how the emission ratios were  
400 determined. For both Apel et al. (2010) and Bon et al. (2011), the authors took the slope of  
401 VOCs versus CO and used different regression techniques and different time periods. Comparing

402 their technique with ours, we generally estimate VOC emission ratios within 50% of the reported  
403 values, and the estimation improves for shorter lived compounds (e.g., aromatics). However, de  
404 Gouw et al. (2017) more carefully took chemistry into consideration for any potential losses of  
405 the VOCs prior to observation to determine emission ratios, similar to this study. We believe the  
406 comparison with de Gouw et al. (2017) provides a more useful comparison in the method  
407 presented here. We find, at most, a 30% difference in the emission ratios, with an average  
408 difference of  $4 \pm 15\%$  for all compounds. Thus, from this analysis, we conclude that (1) there is  
409 large variability in VOC emission ratios across urban areas around the world, which has been  
410 highlighted in other studies (Warneke et al., 2007), and (2) the method that considers losses of  
411 VOCs is the more accurate procedure to estimate VOC emissions and leads to the best  
412 reproducibility across studies and lowest uncertainty ( $< 30\%$ ,  $\sim 4\%$  on average).

## Supporting Information Tables

**Table S1.** List of instruments whose observations are used in this study. In some cases  $\Delta\text{SOA}/\Delta\text{CO}$  (Table S4), SOA versus  $\text{O}_x$  slope (Table S4), or VOC emission ratios (Table S5 through Table S8) had already been reported, and, in those cases, we use the previous literature reports in our analyses.

Location	SOA	$\text{O}_x$	HCHO	PAN	VOCs	CO
Houston, TX, USA (2000)	Q-AMS <sup>a</sup>	CL & UV Absorption <sup>b</sup>	DOAS <sup>c</sup>	GC-ECD <sup>d</sup>	GC-FID, GC-MS <sup>e</sup>	Infrared Absorption <sup>f</sup>
Mexico City, Mexico (2006)	HR-ToF-AMS <sup>g</sup>	CL <sup>h</sup>	TDLAS <sup>i</sup>	CIMS <sup>j</sup>	WAS <sup>k</sup>	UV RF <sup>l</sup>
Los Angeles, CA, USA (2010)	HR-ToF-AMS <sup>g</sup>	CL & UV Absorption <sup>m</sup>	Average of DOAS <sup>c</sup> & Hantzsch Reaction <sup>n</sup>	GC-ECD <sup>d</sup>	GC-MS <sup>o</sup>	UV RF <sup>l</sup>
Beijing, China (2011)	HR-ToF-AMS <sup>g</sup>	CL & UV Absorption <sup>p</sup>	PTR-MS <sup>q</sup>	GC-ECD <sup>r</sup>	GC-FID <sup>s</sup>	IR Absorption <sup>p</sup>
London, UK (2012)	C-ToF-AMS <sup>t</sup>	CL & UV Absorption <sup>u</sup>	Hantzsch Reaction <sup>n</sup>	GC-ECD <sup>v</sup>	GC-FID & GC×GC-FID <sup>w</sup>	UV RF <sup>l</sup>
Houston, TX, USA (2013)	HR-ToF-AMS <sup>g</sup>	CL <sup>x</sup>	Average of LIF <sup>y</sup> & CAMS <sup>z</sup>	CIMS <sup>j</sup>	WAS <sup>k</sup>	DACOM <sup>aa</sup>
Seoul, South Korea (2016)	HR-ToF-AMS <sup>g</sup>	CL <sup>h</sup>	CAMS <sup>z</sup>	CIMS <sup>j</sup>	WAS <sup>k</sup>	DACOM <sup>aa</sup>

<sup>a</sup>Quadrupole Aerosol Mass Spectrometer (Q-AMS) (Jayne et al., 2000)

<sup>b</sup>Chemiluminescence (CL) and UV Absorption (Williams et al., 1997)

<sup>c</sup>Differential Optical Absorption Spectrometry (DOAS) (Stutz and Platt, 1996, 1997)

<sup>d</sup>Gas chromatography-electron capture detector (GC-ECD) (Williams et al., 2000; Roberts et al., 2002)

<sup>e</sup>Gas chromatography-flame ionization detector (GC-FID) and gas chromatography mass spectrometer (Roberts et al., 2001)

<sup>f</sup>TECO Model 48s IR gas-filter

<sup>g</sup>High Resolution Time-of-Flight Aerosol Mass Spectrometer (HR-ToF-AMS) (DeCarlo et al., 2006)

<sup>h</sup>Chemiluminescence (CL) and UV Absorption (Weinheimer et al., 1994)

<sup>i</sup>Tunable diode laser absorption spectroscopic (TDLAS) measurements (Fried et al., 2003)

<sup>j</sup>Chemical ionization mass spectrometer (CIMS) (Huey L Tanner D Slusher D Dibb J Arimoto R Chen G Davis D Buhr M Nowak J Mauldin R Eisele F, 2004; Slusher et al., 2004; Kim et al., 2007)

<sup>k</sup>Whole air sample, followed by analysis with GC-FID and/or GC-MS (Blake et al., 2003)

<sup>l</sup>UV Resonance Fluorescence (RF) (Gerbig et al., 1999)

436 <sup>m</sup>Chemiluminescence (CL) and UV Absorption (Hayes et al., 2013)  
 437 <sup>n</sup>Hantzsch reaction (Cárdenas et al., 2000)  
 438 <sup>o</sup>Gas chromatograph mass spectrometer (Gilman et al., 2010)  
 439 <sup>p</sup>Chemiluminescence (CL), UV Absorption, and IR Absorption (Hu et al., 2016)  
 440 <sup>q</sup>Proton transfer reaction mass spectrometer (PTR-MS) (Warneke et al., 2011)  
 441 <sup>r</sup>Gas chromatography electron capture detector (GC-ECD) (Zhang et al., 2017)  
 442 <sup>s</sup>Gas chromatography flame ionization detector (GC-FID) (Wang et al., 2014)  
 443 <sup>t</sup>Compact Time-of-Flight Aerosol Mass Spectrometer (C-ToF-AMS) (Drewnick et al., 2005)  
 444 <sup>u</sup>Chemiluminescence (CL) and UV Absorption (Whalley et al., 2016)  
 445 <sup>v</sup>Gas chromatography electron capture detector (GC-ECD) (Whalley et al., 2016)  
 446 <sup>w</sup>Gas chromatography flame ionization detector (GC-FID) (Dunmore et al., 2015)  
 447 <sup>x</sup>Chemiluminescence (CL) (Ryerson et al., 1999; Pollack et al., 2010)  
 448 <sup>y</sup>Laser induced fluorescence (LIF) (Cazorla et al., 2015)  
 449 <sup>z</sup>Compact Atmospheric Multi-species Spectrometer (CAMS) difference frequency absorption  
 450 spectrometer (Weibring et al., 2010)  
 451 <sup>aa</sup>Tunable diode laser absorption spectroscopy (Sachse et al., 1987)

452 **Table S2.** Concentrations of PM<sub>1</sub> components shown in Fig. 1. References for the measurements  
 453 can be found in Table 1.

Dataset Location	Average Concentration ( $\mu\text{g sm}^{-3}$ ) of submicron aerosol under standard temperature and pressure				
	SOA	HOA	SO <sub>4</sub>	NO <sub>3</sub>	NH <sub>4</sub>
Houston, TX, USA (2000)	2.7	0.7	4.9	0.4	1.5
Northeast USA (2002)	4.9	0.5	2.0	0.3	0.7
Tokyo, Japan (2004)	6.0	1.5	4.4	0.9	4.0
Mexico City, Mexico (2006)	11.2	4.8	1.9	6.0	2.5
Paris, France (2009)	1.9	1.1	1.2	0.5	0.6
Los Angeles, CA, USA (2010)	5.0	2.0	2.9	3.6	2.1
Changdao Island, China (2011)	9.4	4.4	8.3	12.2	6.5
Beijing, China (2011)	17.1	8.9	22.0	16.8	13.7
London, UK (2012)	2.7	1.6	1.4	2.7	1.3
Houston, TX, USA (2013)	3.7	0.0	2.7	0.1	0.6
New York City, NY, USA (2015)	0.8	0.7	1.2	1.4	0.4
Seoul, South Korea (2016)	11.9	1.3	5.0	7.9	4.4

454

455

456 **Table S3.** Table summarizing the results of recent GEOS-Chem performance evaluations for  
 457 modeling BSOA.

Study	Observed Data	Species	Details
Fisher et al. (2016) <sup>a</sup>	SEAC <sup>4</sup> RS, below 1 km (spatial pattern), below 500 m (bias)	Isoprene	Spatial patterns well captured, and biases are +34% for isoprene and +3% for monoterpenes
		Monoterpene	
		Organic Nitrates from Isoprene	Spatial patterns well captured, and biases are -0.6% for first- and -35% for second-generation isoprene nitrates
	SEAC <sup>4</sup> RS, 0 - 4 km vertical profiles	Isoprene	Agreed well but GEOS-Chem somewhat overestimated observed concentrations near 1km
		Monoterpene	
		HCHO	
	SOAS, at the surface	Organic Nitrates from Isoprene	Agreed within measurement uncertainties
		Isoprene	Underestimated isoprene and monoterpenes (-28% and -54%), but overestimated first- and second- generation isoprene nitrates (+85% and +43%)
		Monoterpene	
		HCHO	
		Organic Nitrates from Isoprene	
Travis et al. (2016)	SEAC <sup>4</sup> RS, 0 - 12 km	First Generation from Isoprene Nitrates	Good agreement for ISOPOOH and ISOPN, underestimation of HPALDs by a factor of two
		ISOPOOH	
		HPALDS	
Marais et al. (2016)	SOAS, at the surface	IEPOX-SOA	Good agreement for isoprene derived aerosols, mean concentrations were almost the same
		ISOPOOH-SOA	
	SEAC <sup>4</sup> RS, below 2 km (spatial pattern)	IEPOX-SOA	Spatial patterns well captured

458 <sup>a</sup>This study decreased isoprene emissions by 15% and doubled monoterpene emissions of  
 459 MEGANv2.1.



460 **Table S3 cont.**

Study	Observed Data	Species	Details
Kaiser et al. (2018) <sup>a</sup>	SEAC <sup>4</sup> RS	Isoprene	All were overestimated, except for first generation isoprene nitrates
		HCHO	
		ISOPOOH	
		MVK + MACR	
		First Generation Isoprene Nitrates	
Pai et al. (2020)	15 airborne campaigns (SEAC <sup>4</sup> RS, GoAmazon, SENEX, OP3, etc.)	OA under biogenic dominant conditions	Slight overestimation, but generally very similar in magnitude

461 <sup>a</sup>NEI NO<sub>x</sub> emissions other than power plants decreased by 60%, soil NO<sub>x</sub> emissions were  
 462 reduced by 50% across the Midwestern US. With the decrease of NO<sub>x</sub> emissions, ISOPOOH  
 463 concentrations were increased in GEOS-Chem.

**Table S4.** Dilution-corrected SOA concentrations at 0.5 equivalent days and slopes of SOA versus O<sub>x</sub>, HCHO, and PAN used in Fig. 2 and Fig. 3. References for the values can be found either in Table 1 or found in Fig. S2 through Fig. S4. Uncertainty is 1σ, and either represents propagation in uncertainty in measurements (see Sect. S5) for ΔSOA/ΔCO or uncertainty in slopes for SOA versus the three photochemical species.

Dataset Location	ΔSOA/ΔCO at 0.5 eq. days	SOA vs. O <sub>x</sub> Slopes	SOA vs. HCHO Slopes	SOA vs. PAN Slopes
Houston, TX, USA (2000)		0.04±0.01 <sup>a</sup>	0.32±0.08	1.41±0.46
Northeast USA (2002)	16±3 <sup>b</sup> 48±9 <sup>c</sup>			
Mexico City, Mexico (2003)		0.14±0.01 <sup>a</sup>		
Tokyo, Japan (2004)		0.19±0.01 <sup>a</sup>		
Mexico City, Mexico (2006)	58±10	0.16±0.01	1.60±0.06	5.60±0.30
Paris, France (2009)		0.14±0.01 <sup>a</sup>		
Pasadena, CA, USA (2010)	59±11	0.16±0.01	1.93±0.02	5.41±0.12
Changdao Island, China (2011)	23±4			
Beijing, China (2011)	31±6	0.21±0.01	3.90±0.15	7.42±0.46
London, UK (2012)	54±10	0.13±0.01	0.36±0.02	3.37±0.41
Houston, TX, USA (2013)		0.16±0.01	1.52±0.13	6.92±0.58
New York City, NY, USA (2015)	33±6			
Seoul, South Korea (2016)	107±19	0.29±0.02	3.73±0.26	10.13±0.52

<sup>a</sup>Missing reported uncertainty; therefore, assuming ±0.01, as that is typical for other campaigns

<sup>b</sup>From de Gouw et al. (2005). <sup>c</sup>From Kleinman et al. (2007).

471 **Table S5.** Emission ratios of BTEX aromatics used in this study. If no reference is listed, then  
 472 the emission ratio was calculated using Eq. 3.

Dataset Location	Emission Ratios (ppbv aromatic/ppmv CO)					References
	Benzene	Toluene	Ethylbenzene	m+p-xylene	o-xylene	
Houston, TX, USA (2000)	2.6	3.5	0.6	2.8	0.8	
NE USA, Ship (2002)	0.9	2.0	0.2	0.6	0.3	Baker et al. (2008)
NE USA, Aircraft (2002)	0.8	2.9	0.4	1.2	0.5	Warneke et al. (2007)
Mexico City, Mexico (2006)	0.9	7.5	0.9	1.1	0.4	Apel et al. (2010)
Los Angeles, CA, USA (2010)	1.3	3.4	0.6	2.1	0.8	de Gouw et al. (2017)
Changdao Island, China (2011)	2.3	1.9	0.5	1.3	0.4	Yuan et al. (2013)
Beijing, China (2011)	1.2	2.4	1.0	1.6	0.6	Wang et al. (2014)
London, UK (2012)	1.8	6.3	1.2	2.2	1.1	
Houston, TX, USA (2013)	2.3	3.0	0.6	3.9	1.2	
New York City, NY, USA (2015)	0.8	2.9	0.4	1.2	0.5	Warneke et al. (2007) <sup>a</sup>
Seoul, South Korea (2016)	1.1	13.1	2.4	3.3	2.3	

473 <sup>a</sup>Using the emissions from Warneke et al. (2007) instead of Schroder et al. (2018) as Schroder et  
 474 al. found significant uncertainty in the emissions calculated from observations.

475 **Table S6.** Emission ratios of alkanes used in this study. If no reference is listed, then the  
 476 emission ratio was calculated using Eq. 3.

Dataset Location	Emission Ratios (ppbv alkane/ppmv CO)							References
	Ethane	Propane	n-Butane	i-Butane	n-Pentane	i-Pentane	n-Hexane	
Houston, TX, USA (2000)	40.9	24.3	9.0	14.7	3.1	10.0	3.1	
NE USA, Ship (2002)	8.3	2.3	1.8	1.3	1.0	2.8	0.9	Baker et al. (2008)
NE USA, Aircraft (2002)	9.9	9.0	2.4	1.3	2.0	5.4	0.6	Warneke et al. (2007)
Mexico City, Mexico (2006)	7.4	41.5	15.1	4.8	2.1	2.7	1.5	Apel et al. (2010)
Los Angeles, CA, USA (2010)	16.5	13.4	5.0	3.2	3.4	8.7	1.4	de Gouw et al. (2017)
Changdao Island, China (2011)	7.7	4.5	2.5	1.2	1.0	1.5	0.5	Yuan et al. (2013)
Beijing, China (2011)	4.3	3.9	2.5	2.5	1.2	2.0	0.6	Wang et al. (2014)
London, UK (2012)	33.0	17.8	17.3	8.4	4.6	11.3	1.3	
Houston, TX, USA (2013)	86.5	37.3	14.6	10.6	7.0	10.5	3.0	
Seoul, South Korea (2016)	16.1	0.4	6.0	3.4	3.1	3.7	1.7	

477

478 **Table S7.** Emission ratios of alkenes used in this study. If no reference is listed, then the  
 479 emission ratio was calculated using Eq. 3.

Dataset Location	Emission Ratios (ppbv alkene/ppmv CO)		References
	Ethene	Propene	
Houston, TX, USA (2000)	24.4	28.4	
NE USA, Ship (2002)	4.4	1.1	Baker et al. (2008)
NE USA, Aircraft (2002)	4.9	1.4	Warneke et al. (2007)
Mexico City, Mexico (2006)	8.4	2.6	Apel et al. (2010)
Los Angeles, CA, USA (2010)	11.2	4.1	de Gouw et al. (2017)
Changdao Island, China (2011)	5.3	1.4	Yuan et al. (2013)
Beijing, China (2011)	4.4	1.4	Wang et al. (2014)
London, UK (2012)	10.3	6.2	
Houston, TX, USA (2013)	12.0	15.8	
Seoul, South Korea (2016)	5.4	2.1	

480

481 **Table S8.** Emission ratios of non-BTEX aromatics used in this study. If no reference is listed,  
 482 then the emission ratio was calculated using Eq. 3.

Dataset Location	Emission Ratios (ppbv aromatic/ppmv CO)			References
	Trimethylbenzenes	Ethyltoluenes	Propylbenzene	
NE USA, Aircraft (2002)	0.71	0.58	0.14	Warneke et al. (2007)
Los Angeles, CA, USA (2010)	1.47	0.56	0.13	de Gouw et al.(2017)
Beijing, China (2011)	0.57	0.41	0.09	Wang et al. (2014)
London, UK (2012)	0.49	0.23	0.58	
New York City, NY, USA (2015)	0.71	0.58	0.14	Warneke et al. (2007)

483

484

485 **Table S9.** Normalized mass concentration of primary organic aerosol (POA/CO) measured in  
 486 various campaigns, used to determine SVOC emission ratios.

Dataset Location	Normalized Mass Concentration ( $\mu\text{g sm}^{-3}$ ppmv <sup>-1</sup> )		References
	HOA/CO	Other POA/CO	
NE USA (2002)	12.2	-	de Gouw et al. (2005)
Los Angeles, CA, USA (2010)	5.3	7.7	Hayes et al. (2013)
Beijing, China (2011)	6.1	9.9	Hu et al. (2016)
London, UK (2012)	17.9	14.1	Young et al. (2015)
New York City, NY, USA (2015)	5.6	14.4	Schroder et al. (2018)

487

**Table S10.** Comparison of estimated VOC emission ratios from two studies from Mexico City (Apel et al., 2010; Bon et al., 2011), one study from Los Angeles (de Gouw et al., 2017), and this study.

VOC Ratio	Apel et al. (2010) Downtown MC	This Study	Apel et al. (2010) Suburbs MC	Bon et al. (2011) Outskirt MC	This Study	de Gouw et al. (2017) LA	This Study
Ethane	7.4	8.2	3.0	21.5	8.2	16.5	18.9
Propane	41.5	36.9	49.3	61.7	38.4	13.4	14.0
n-Butane	15.1	14.9	15.3	21.7	14.1	5.0	5.7
i-Butane	4.8	4.8	5.3	7.2	4.9	3.2	3.5
n-Pentane	2.1	2.9	2.1	2.5	2.1	3.4	3.4
i-Pentane	2.7	3.6	3.2	3.3	3.1	8.7	7.8
n-Hexane	1.5	1.9	1.3	1.5	1.2	1.4	1.7
Ethene	8.4	6.1	7.9	7.0	7.1	11.2	9.6
Propene	2.6	1.3	2.9	3.0	1.6	4.1	3.9
Benzene	0.9	1.0	1.2	1.2	1.3	1.3	1.4
Toluene	7.5	9.2	5.2	4.2	4.1	3.4	3.0
Ethylbenzene	0.9	0.8	0.4	4.3*	0.4	0.6	0.6
m+p-Xylene	1.1	0.7	0.5	No Data	0.4	2.1	1.9
o-Xylene	0.4	0.2	0.2	No Data	0.2	0.8	0.7
Trimethylbenzenes	No Data	No Data	No Data	No Data	No Data	1.6	1.1
Ethyltoluenes	No Data	No Data	No Data	No Data	No Data	0.6	0.4
Propylbenzene	No Data	No Data	No Data	No Data	No Data	0.1	0.1

\*In Bon et al. (2011), they reported the sum of C8 aromatics, which is the sum of ethylbenzene and xylenes

493 **Table S11.** Statistical analysis of the data used in Fig. 2 to determine if any point is influencing  
 494 the slope, using the T-test, Cook's Distance test, and Difference in Fits test. For the T-test, the  
 495 point is influential if the t value is  $< 0.05$  while for the Cook's Distance and Difference in Fits  
 496 test, the point is influential if the value is  $> 1$ .

Campaign	T-test	Cook's Distance	Difference in Fits
NE US Ship	0.63	0.06	-0.29
NE US Aircraft	0.12	0.27	0.73
Mexico City	0.39	0.06	0.33
Los Angeles	0.32	0.08	0.38
Changdao Island, China	0.41	0.09	-0.38
Beijing	0.42	0.06	-0.32
London	0.31	0.13	-0.48
NYC	0.90	0.00	-0.05
Seoul	0.99	0.00	0.01

497



498 **Table S12.** Rate constants used throughout this study.

Compound	Rate Constant (cm <sup>3</sup> molec. <sup>-1</sup> s <sup>-1</sup> )	References
<i>Alkanes</i>		
Ethane	$6.9 \times 10^{-12} \times \exp(-1000/T)$	Atkinson et al. (2006)
Propane	$7.6 \times 10^{-12} \times \exp(-585/T)$	Atkinson et al. (2006)
n-Butane	$9.8 \times 10^{-12} \times \exp(-425/T)$	Atkinson et al. (2006)
i-Butane	$1.17 \times 10^{-17} \times T^2 \times \exp(213/T)$	Atkinson and Arey (2003)
n-Pentane	$2.52 \times 10^{-17} \times T^2 \times \exp(158/T)$	Atkinson and Arey (2003)
i-Pentane	$3.6 \times 10^{-12}$	Atkinson and Arey (2003)
n-Hexane	$2.54 \times 10^{-14} \times T \times \exp(-112/T)$	Atkinson and Arey (2003)
<i>Alkenes</i>		
Ethene	$7.84 \times 10^{-12,a}$	Atkinson et al. (2006)
Propene	$2.86 \times 10^{-11,a}$	Atkinson et al. (2006)
<i>Aromatics</i>		
Benzene	$2.3 \times 10^{-12} \times \exp(-190/T)$	Atkinson et al. (2006)
Toluene	$1.8 \times 10^{-12} \times \exp(340/T)$	Atkinson et al. (2006)
Ethylbenzene	$7 \times 10^{-12}$	Atkinson and Arey (2003)
m+p-xylene	$1.87 \times 10^{-11,b}$	Atkinson and Arey (2003)
o-xylene	$1.36 \times 10^{-11}$	Atkinson and Arey (2003)
Trimethylbenzenes	$2.73 \times 10^{-12} \times \exp(730/T)$	Bohn and Zetzsch (2012)
Ethyltoluenes	$1.2 \times 10^{-11}$	Atkinson and Arey (2003)
Propylbenzene	$5.8 \times 10^{-12}$	Atkinson and Arey (2003)
<i>S/IVOCs</i>		
IVOCs C* = 4 - 6	$2 \times 10^{-11}$	Jathar et al. (2014)
IVOCs C* = 3	$3 \times 10^{-11}$	McDonald et al. (2018)
SVOCs & “aging”	$4 \times 10^{-11}$	Tsimpidi et al. (2010)
<i>NO<sub>x</sub>/NO<sub>y</sub></i>		
OH + NO <sub>2</sub>	$1.23 \times 10^{-11,a}$	Mollner et al. (2010)

499 <sup>a</sup>Showing the rate constant at 298 K, 1013 hPa. However, for this study, we used the temperature  
500 and pressure dependent formulation listed in each respective reference.  
501 <sup>b</sup>This is the average of m-xylene and p-xylene rate constants.

**Table 13.** Parameters for VOC, IVOC, and SVOC aerosol yields. The yields are taken from Ma et al. (2017).

Compound	Stoichiometric SOA yield High-NO <sub>x</sub> , 298 K (μg m <sup>-3</sup> )				
	0.1	1	10	100	1000
Benzene					
Toluene					
Ethyltoluene	N/A	0.276	0.002	0.431	0.202
Propylbenzenes					
Xylenes					
Trimethylbenzenes	N/A	0.310	0.000	0.420	0.209
IVOC C* = 6	0.007	0.090	0.206	0.350	0.00
IVOC C* = 5	0.0498	0.0814	0.456	0.278	0.00
IVOC C* = 4	0.053	0.103	0.464	0.266	0.00
IVOC C* = 3	0.064	0.0914	0.562	0.209	0.00
HOA C* = 2	N/A	N/A	0.28	N/A	N/A
HOA C* = 1	N/A	0.18	N/A	N/A	N/A
HOA C* = 0	0.12	N/A	N/A	N/A	N/A
COA C* = 2	N/A	N/A	0.1881	N/A	N/A
COA C* = 1	N/A	0.1188	N/A	N/A	N/A
COA C* = 0	0.0594	N/A	N/A	N/A	N/A

504

505 **Table S14.** Table of GBD parameters, which is the mean of the draw values (see associated file)  
 506 from the IHME website:  
 507 [http://ghdx.healthdata.org/record/global-burden-disease-study-2010-gbd-2010-ambient-air-pollut](http://ghdx.healthdata.org/record/global-burden-disease-study-2010-gbd-2010-ambient-air-pollution-risk-model-1990-2010)  
 508 [ion-risk-model-1990-2010](http://ghdx.healthdata.org/record/global-burden-disease-study-2010-gbd-2010-ambient-air-pollution-risk-model-1990-2010).

Parameter	IHD	Stroke	COPD	LC	ALRI
$\alpha$	1.4273	1.2641	15.224	114.74	2.2023
$\beta$	0.04764	0.00722	0.00095	0.000141	0.000284
$\rho$	0.376	1.314	0.684	0.741	1.183
PM <sub>2.5,Threshold</sub>	7.462	7.387	7.374	7.380	7.283

509

510 **Table S15.** Table of GEMM parameters. The GEMM parameters are from Burnett et al. (2018),  
511 with the Chinese male cohort.

Cause of Death	Age Range (years)	$\theta$	Standard Error $\theta$	$\alpha$	$\mu$	$\pi$
NCD + LRI	>25	0.1430	0.01807	1.6	15.5	36.8
	27.5	0.1585	0.01477	1.6	15.5	36.8
	32.5	0.1577	0.01470	1.6	15.5	36.8
	37.5	0.1570	0.01463	1.6	15.5	36.8
	42.5	0.1558	0.01450	1.6	15.5	36.8
	47.5	0.1532	0.01425	1.6	15.5	36.8
	52.5	0.1499	0.01394	1.6	15.5	36.8
	57.5	0.1462	0.01361	1.6	15.5	36.8
	62.5	0.1421	0.01325	1.6	15.5	36.8
	67.5	0.1374	0.01284	1.6	15.5	36.8
	72.5	0.1319	0.01234	1.6	15.5	36.8
	77.5	0.1253	0.01174	1.6	15.5	36.8
	85	0.1141	0.01071	1.6	15.5	36.8
	>25	0.2969	0.01787	1.9	12	40.2
IHD	27.5	0.5070	0.02458	1.9	12	40.2
	32.5	0.4762	0.02309	1.9	12	40.2
	37.5	0.4455	0.02160	1.9	12	40.2
	42.5	0.4148	0.02011	1.9	12	40.2
	47.5	0.3841	0.01862	1.9	12	40.2
	52.5	0.3533	0.01713	1.9	12	40.2
	57.5	0.3226	0.01564	1.9	12	40.2
	62.5	0.2919	0.01415	1.9	12	40.2

512

513 **Table 15 cont.**

<b>Cause of Death</b>	<b>Age Range (years)</b>	<b><math>\theta</math></b>	<b>Standard Error <math>\theta</math></b>	<b><math>\alpha</math></b>	<b><math>\mu</math></b>	<b><math>\pi</math></b>
IHD	67.5	0.2612	0.01266	1.9	12	40.2
	72.5	0.2304	0.01117	1.9	12	40.2
	77.5	0.1997	0.00968	1.9	12	40.2
	85	0.1536	0.00745	1.9	12	40.2
Stroke	>25	0.2720	0.07697	6.2	16.7	23.7
	27.5	0.4513	0.11919	6.2	16.7	23.7
	32.5	0.4240	0.11197	6.2	16.7	23.7
	37.5	0.3966	0.10475	6.2	16.7	23.7
	42.5	0.3693	0.09752	6.2	16.7	23.7
	47.5	0.3419	0.09030	6.2	16.7	23.7
	52.5	0.3146	0.08307	6.2	16.7	23.7
	57.5	0.2872	0.07585	6.2	16.7	23.7
	62.5	0.2598	0.06863	6.2	16.7	23.7
	67.5	0.2325	0.06190	6.2	16.7	23.7
	72.5	0.2051	0.05418	6.2	16.7	23.7
	77.5	0.1778	0.04695	6.2	16.7	23.7
	85	0.1368	0.03611	6.2	16.7	23.7
COPD	>25	0.2510	0.06762	6.5	2.5	3.2
Lung Cancer	>25	0.2942	0.06147	6.2	9.3	29.8
LRI	>25	0.4468	0.11735	6.4	5.7	8.4

514

515 **Table S16.** Calculated premature mortality from PM with all aerosol (base mortality) and  
 516 removing ASOA, using the IER method.

Location <sup>a</sup>	Base Mortality	Mortality reduced due to removing ASOA	Percent mortality reduced due to removing ASOA
North America	43,408	18,479	43%
Central America	11,808	3,395	29%
South America	31,214	10,100	32%
Africa	258,294	14,869	6%
Western Europe	305,754	31,880	10%
Eastern Europe	195,749	16,003	8%
South Asia	938,967	75,085	8%
Southeastern Asia	135,433	31,886	24%
East Asia	1,315,720	122,190	9%
Oceania	95	27	28%
Rest of the World	72,385	13,337	18%
Total	3,308,957	337,224	10%

517 <sup>a</sup>Locations defined by:

518 [http://themasites.pbl.nl/tridion/en/themasites/\\_disabled\\_image/background/regions/index-2.html](http://themasites.pbl.nl/tridion/en/themasites/_disabled_image/background/regions/index-2.html)

519 **Table S17.** Calculated premature mortality from PM with all aerosol (base mortality) and  
520 removing ASOA, using the GEMM method.

Location <sup>a</sup>	Base Mortality	Mortality reduced due to removing ASOA	Percent mortality reduced due to removing ASOA
North America	178,793	24,892	14%
Central America	58,516	7,298	12%
South America	145,395	22,372	15%
Africa	765,946	34,528	5%
Western Europe	768,991	50,427	7%
Eastern Europe	465,341	25,552	5%
South Asia	2,285,903	166,228	7%
Southeastern Asia	347,191	50,802	15%
East Asia	2,487,349	220,264	9%
Oceania	3,375	428	13%
Rest of the World	269,769	35,051	13%
Total	7,776,570	638,219	8%

521 <sup>a</sup>Locations defined by:

522 [http://themasites.pbl.nl/tridion/en/themasites/\\_disabled\\_image/background/regions/index-2.html](http://themasites.pbl.nl/tridion/en/themasites/_disabled_image/background/regions/index-2.html)

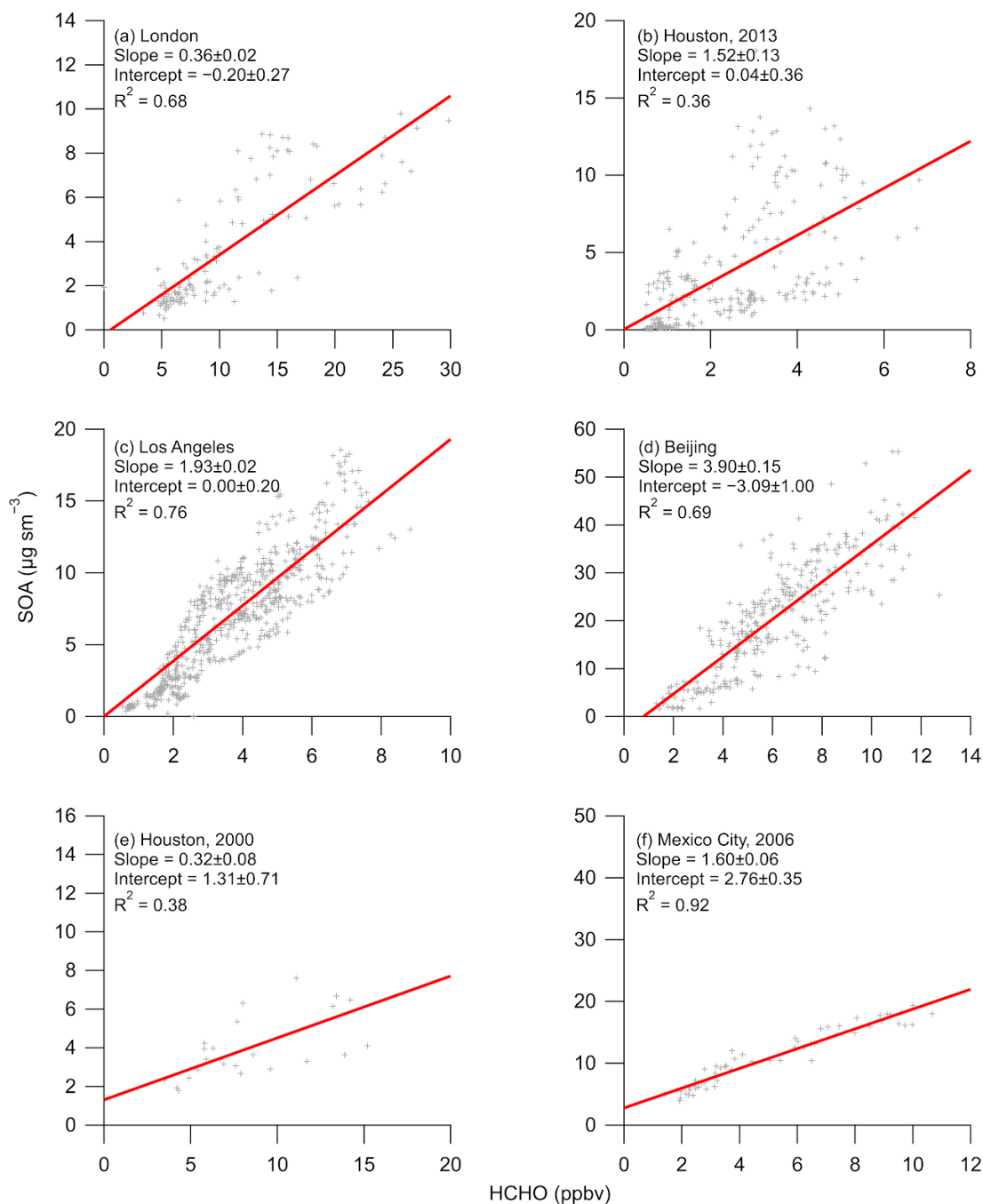


523 **Table S18.** List of total final consumption, in millions of tonnes of oil equivalent, of oil products  
524 and oil, for each organization. Total final consumption includes imports, and does not include  
525 exports (IEA, 2019).

Organization	Industry	Transportation	Non-Energy
World	307	2533	645
OECD	89	1147	326
Africa	18.4	115.4	7.9
Non-OECD	28.3	135	20
Middle East	33.5	126.3	47.5
Non-OECD Europe and Eurasia	35	101	53

526

## 527 Supplemental figures for this study



529 **Figure S1.** Regression plot of SOA versus HCHO from different campaigns around the world  
 530 that have not been previously published. Note, for (c), HCHO is  $1.24 \times$  Hantzsch HCHO, to  
 531 account for the differences between the two HCHO measurements during CalNex. Note, for (a),  
 532 SOA is  $0.5 \times$  OA, estimated from Young et al. (2015), and for (f), SOA is  $0.8 \times$  OA, estimated from  
 533 DeCarlo et al. (2010).

534

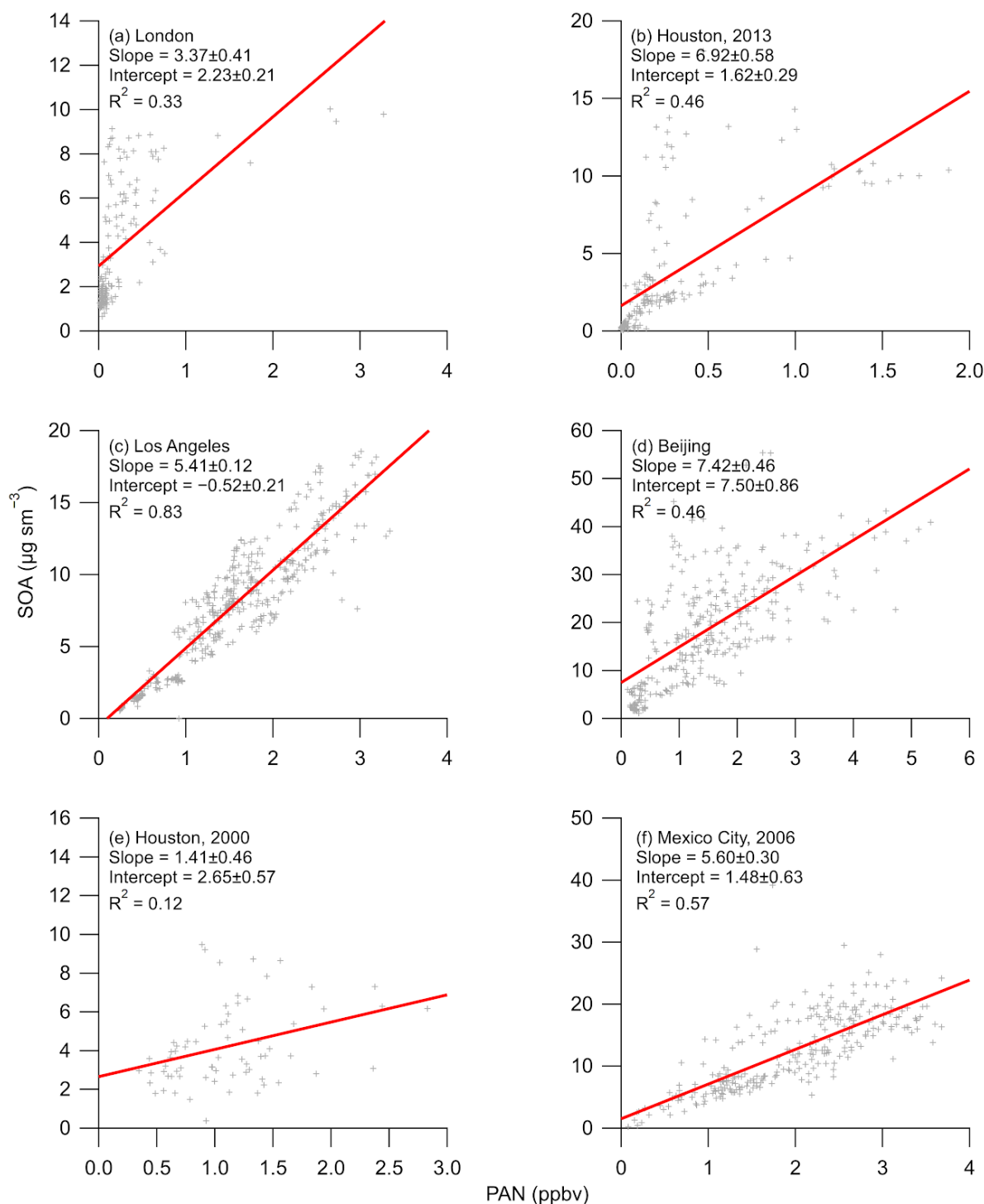
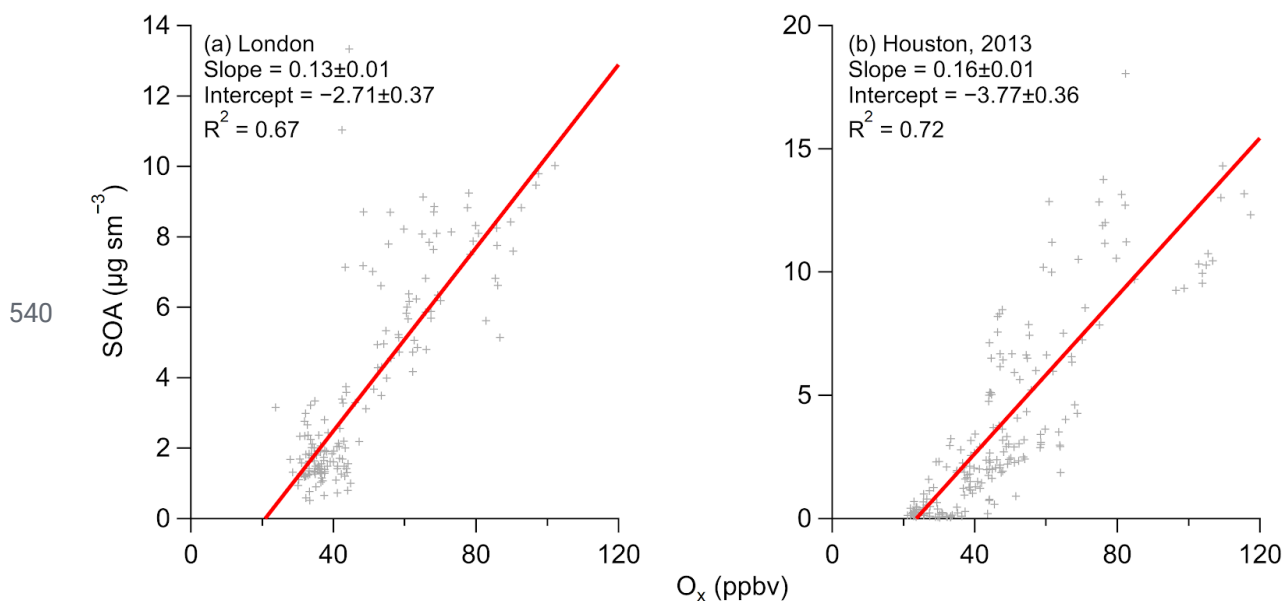
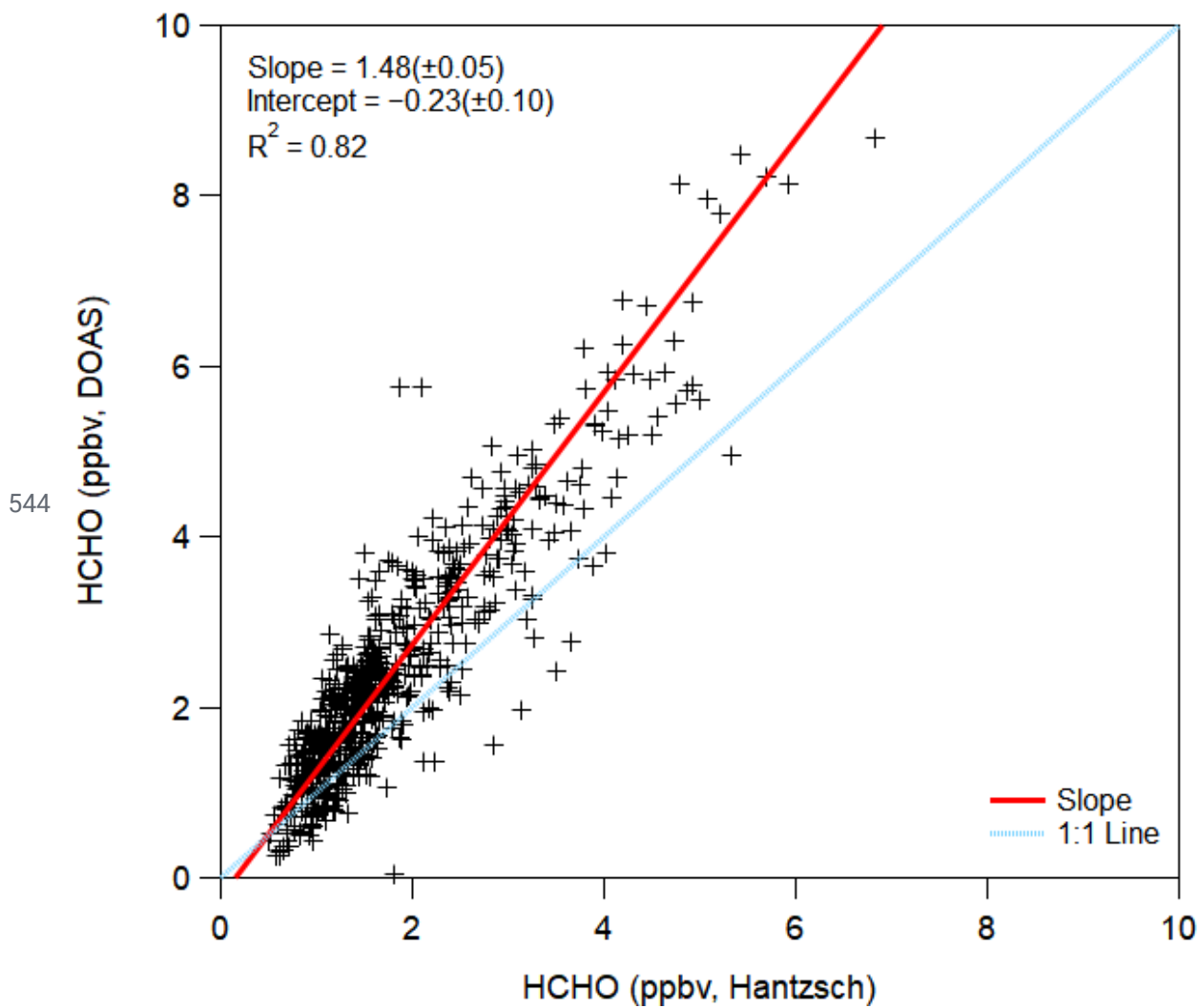


**Figure S2.** Regression plot of SOA versus PAN from different campaigns around the world that have not been previously published. Note, for (a), SOA is  $0.5 \times \text{OA}$ , estimated from Young et al. (2015), and for (f), SOA is  $0.8 \times \text{OA}$ , estimated from DeCarlo et al. (2010).

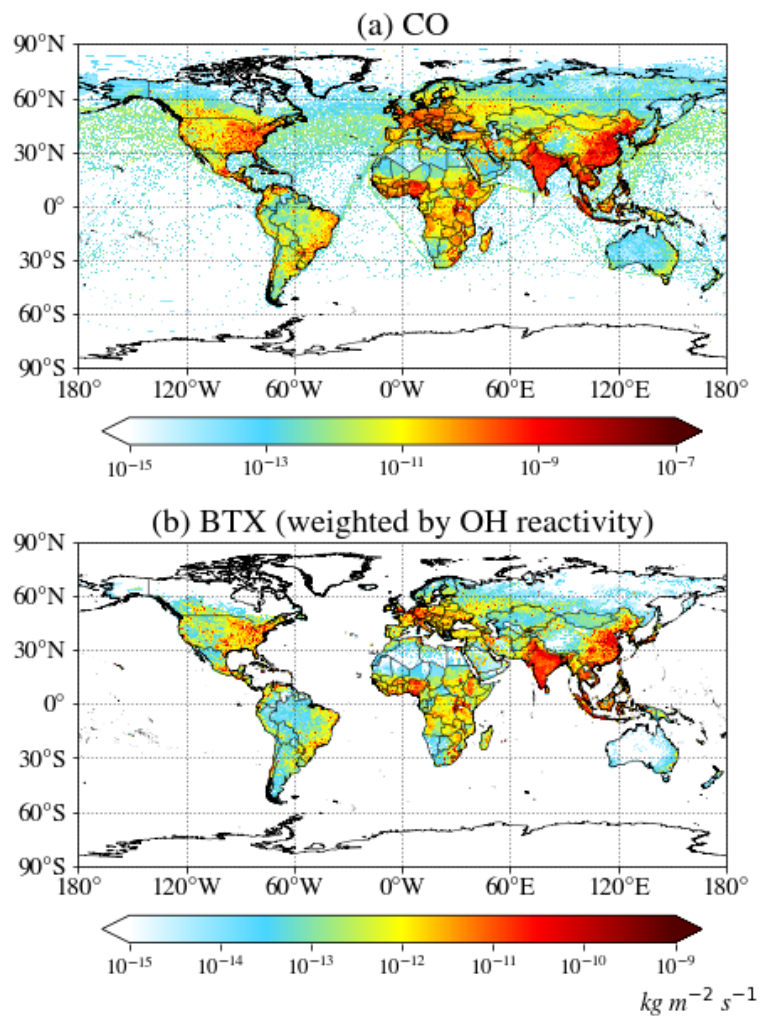
539



541 **Figure S3.** Regression plot of SOA versus  $O_x$  from different campaigns around the world that  
 542 have not been previously published. Note, for (a), SOA is  $0.5 \times \text{OA}$ , estimated from Young et al.  
 543 (2015).



545 **Figure S4.** Comparison of HCHO measured by the DOAS (Stutz and Platt, 1996, 1997) and  
 546 Hantzsch reaction (Cárdenas et al., 2000) methods during the CalNex 2010 study in Pasadena,  
 547 CA, ground site (Ryerson et al., 2013).



548

549 **Figure S5.** (a) Annually average CO emissions from HTaP. (b) Annually average benzene,  
 550 toluene, and xylenes (BTX) emissions, weighted by their OH reaction rate

551 
$$(E_{weight} = N \frac{\sum_i E_i k_{OH,i}}{\sum_i k_{OH,i}}, i = B, T, X; N=3).$$

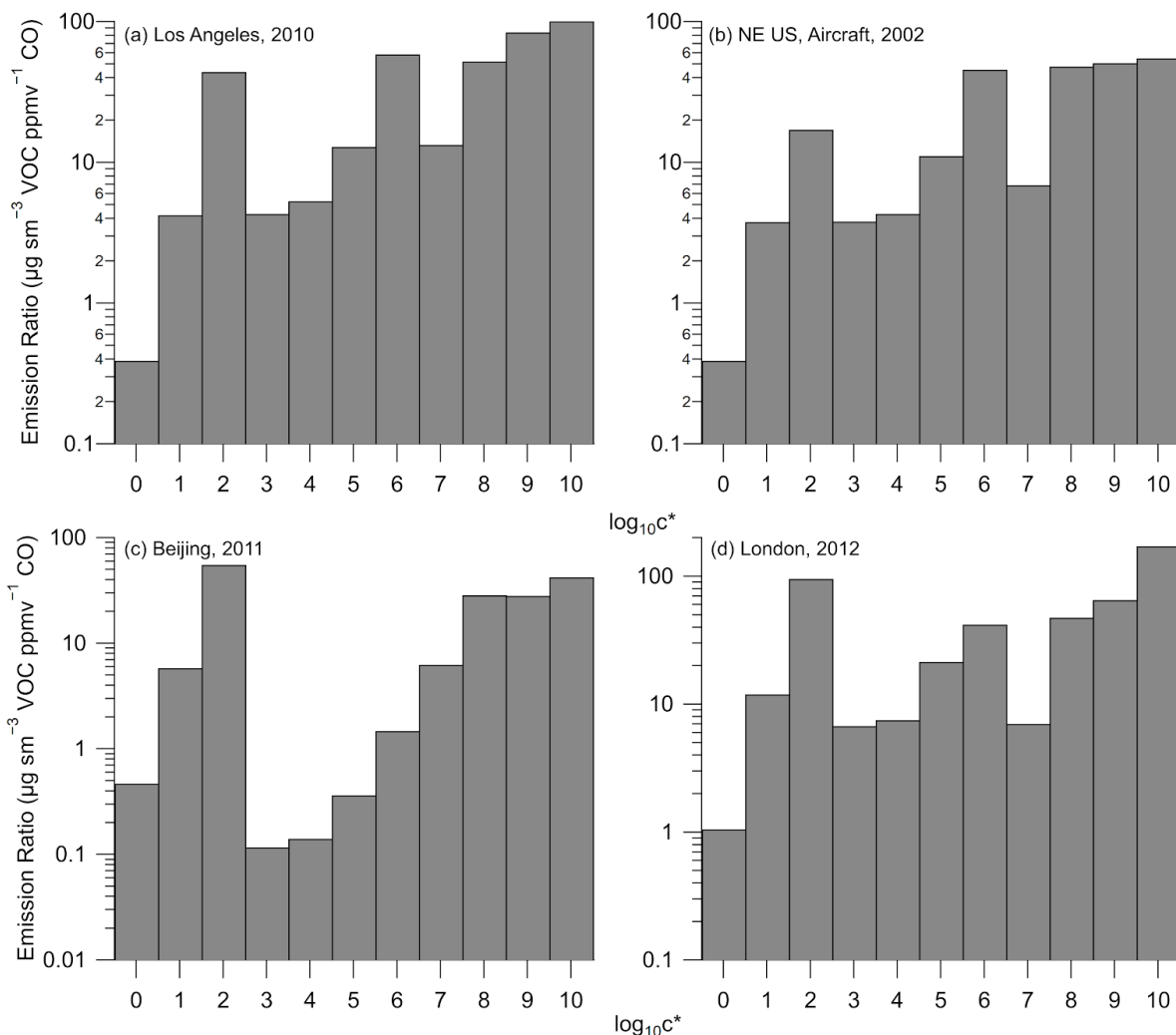


**Figure S6.** Emission ratio versus saturation concentration ( $\log_{10}(c^*)$ ) for (a) Los Angeles, (b) NE US, aircraft, (c) Beijing, and (d) London. The emission ratios for VOCs ( $\log_{10}(c^*) \geq 7$ ) were taken from de Gouw et al. (2017) and Ma et al. (2017) for Los Angeles, Warneke et al. (2007) for NE US, aircraft, and Wang et al. (2014) for Beijing while the VOC emission ratio for London is from Table S6 to Table S8. For VOCs between  $\log_{10}(c^*)$  of 3 and 6 (IVOCs), the volatility distribution from McDonald et al. (2018), along with the ratio of IVOC to BTEX from Figure SI-6 and the emission ratio of BTEX (Table S6), were used to determine the emission ratio versus saturation concentration. Finally, for VOCs between  $\log_{10}(c^*)$  0 and 2 (SVOCs), the volatility distributions from Robinson et al. (2007) for non-fossil fuel POA and from Worton et al. (2014) for fossil fuel POA were used to convert the normalized POA mass concentration (Table S9) to VOC emission ratios. Note, the emission ratio versus saturation concentration for New York City, 2015, was similar to (b), as the emissions were similar (Fig. 5) and the BTEX for New York City is the same as NE US (Table S5).

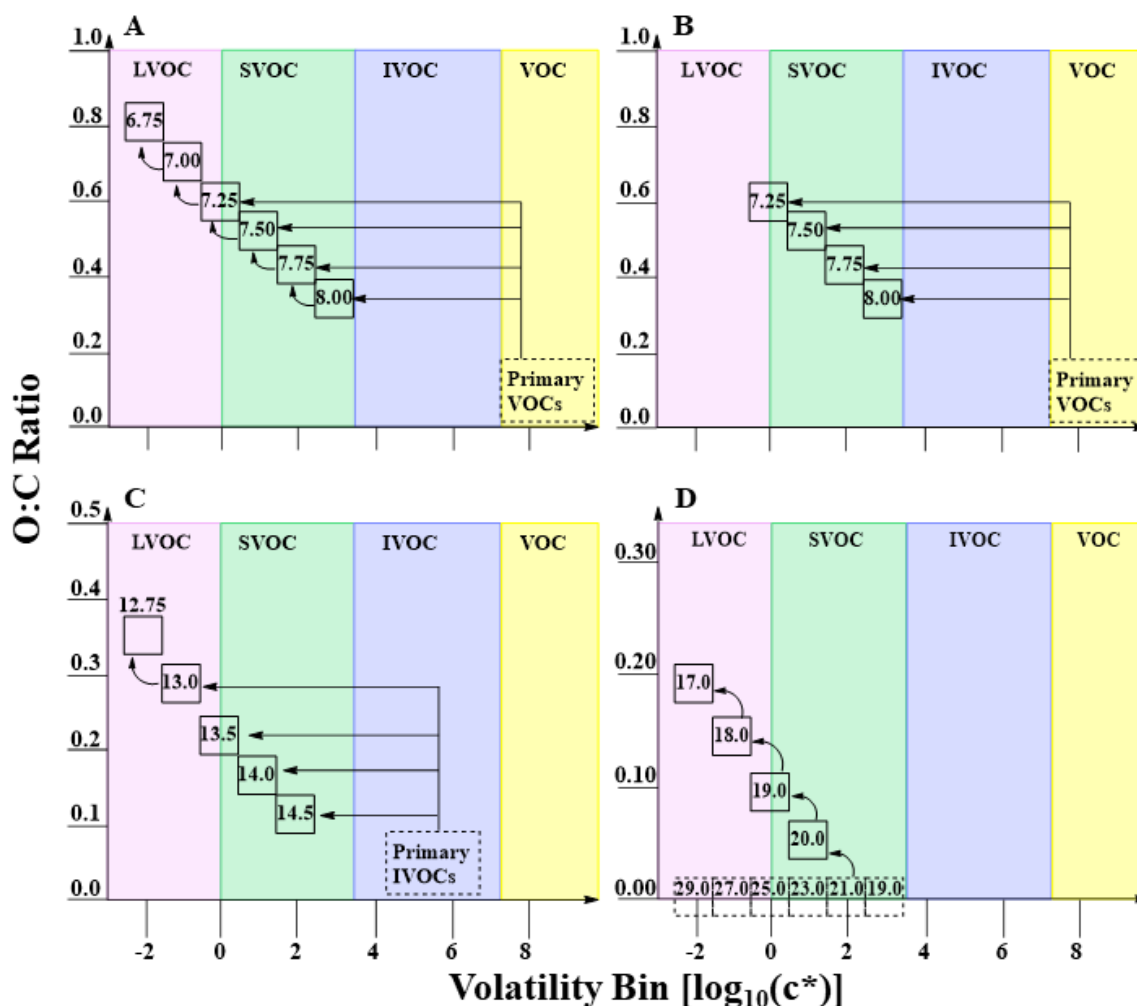
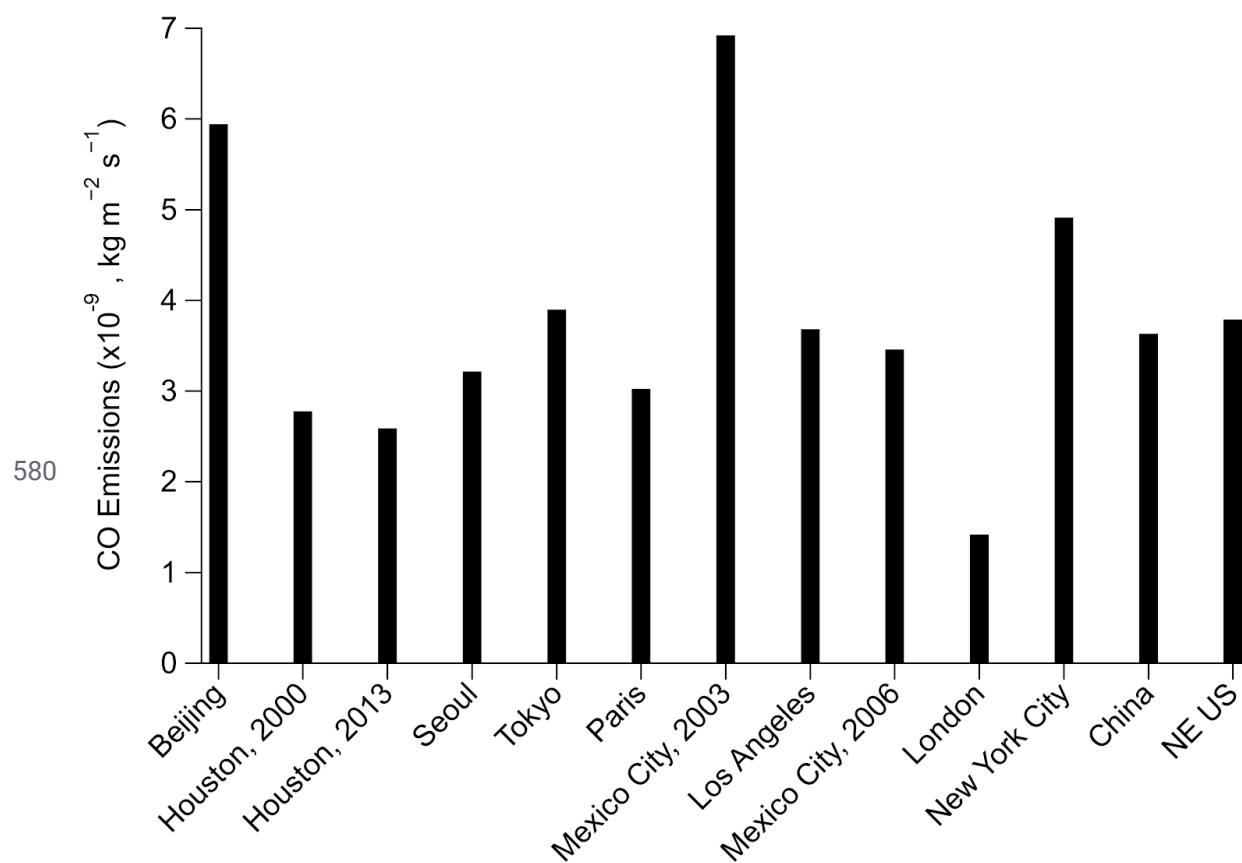
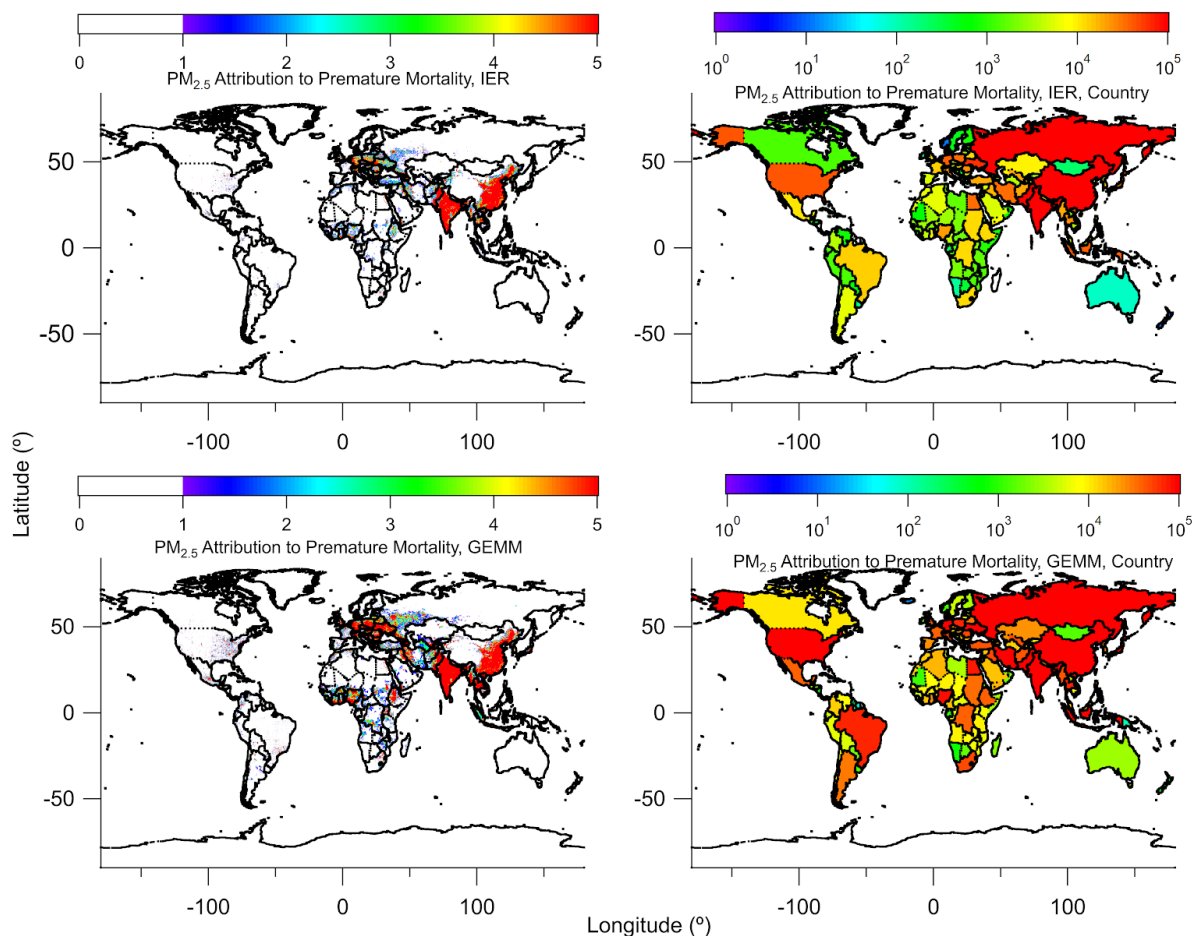


**Figure S7.** 2-D VBS space defined by oxygen to carbon (O:C) ratio and saturation concentration  $[\log_{10}(c^*)]$  for different oxidation mechanisms and primary sources of OA precursors. Dashed boxes represent primary emissions, while the full boxes represent the secondary oxidation products. (A) and (B) represent different parameterizations for treating traditional anthropogenic and biogenic sources of SOA. Both parameterizations depict the oxidation of an 8-carbon precursor VOC. (A) represents the TSI, or aging, parameterization; (B) represents the MA, or wall-loss corrected, parameterization. (C) Represents the initial oxidation and aging pathway of P-IVOCs following the ZHAO parameterization. It should be noted that the carbon number corresponds to first generation aging and subsequent oxidation results in a 0.25 reduction in carbon number. (D) Represents the decadal aging of SVOCs by hydroxyl radicals. In (D), the full aging pathway of only the C21 species is depicted as an example, though all primary species are allowed to age until the  $\log_{10}(c^*) = -2$  bin. All emitted P-SVOC species undergo the same decadal aging scheme which begins from the saturation concentration bin of the emitted species.

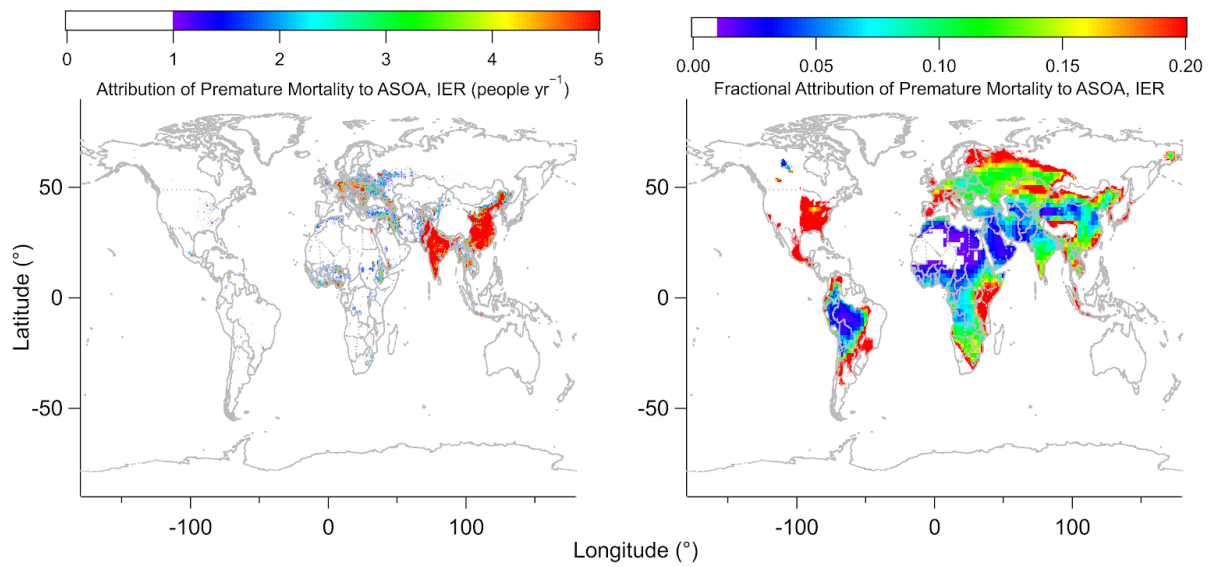




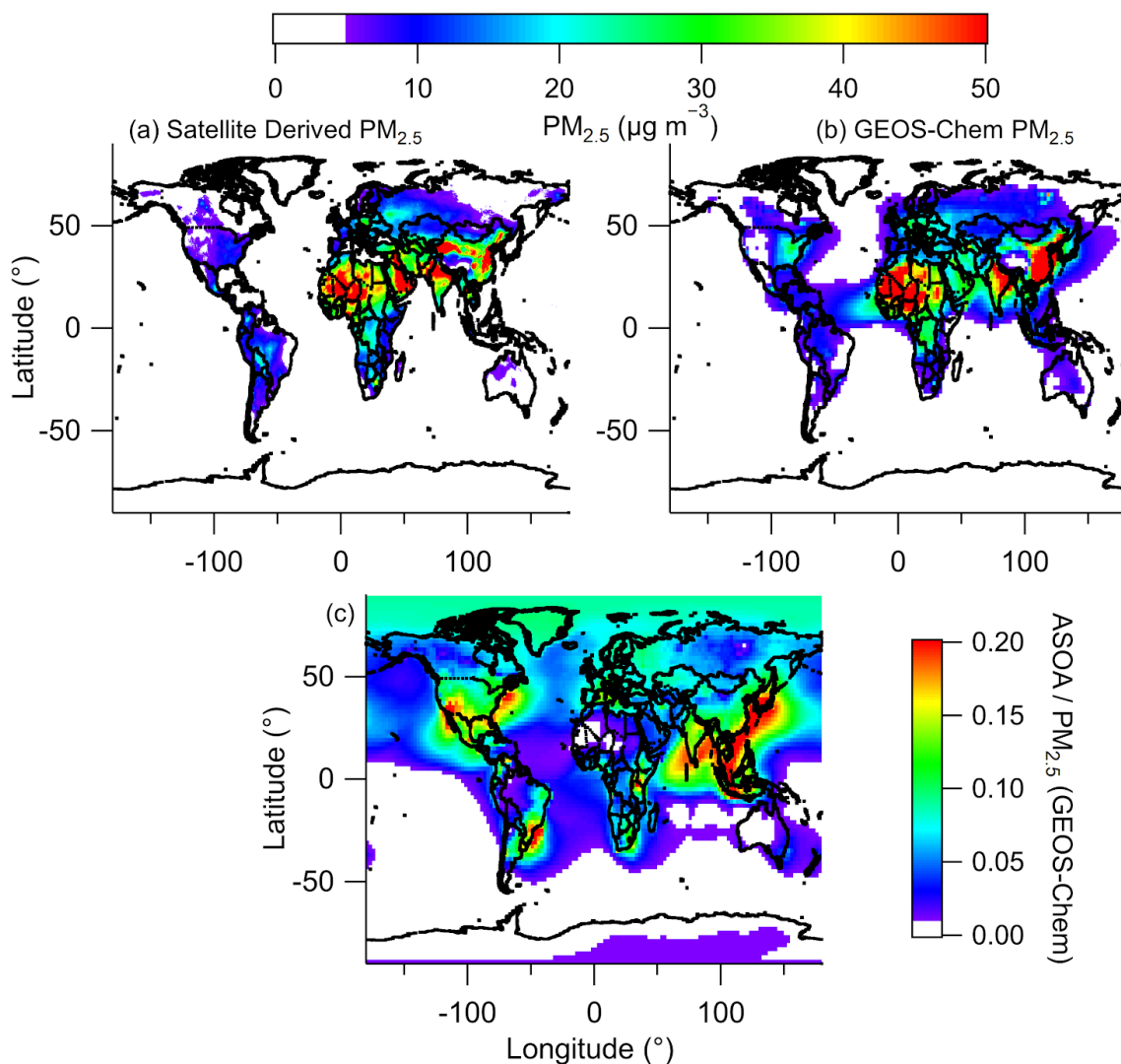
581 **Figure S8.** CO emissions for the cities investigated here from HTAP (Janssens-Maenhout et al.,  
 582 2015).



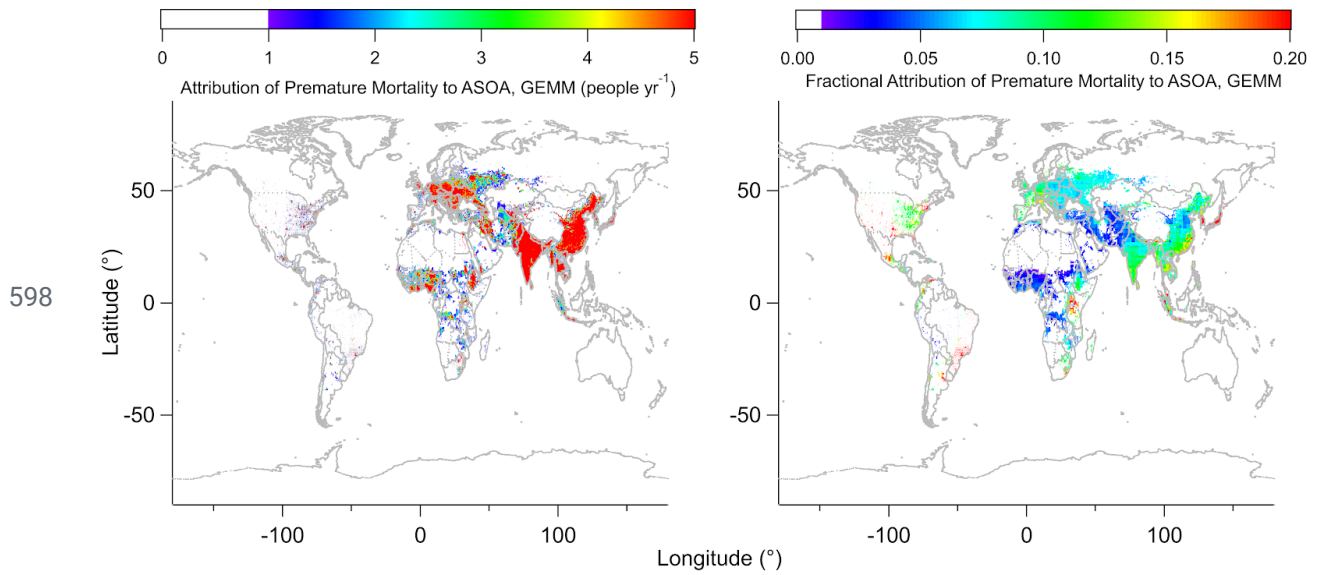
**Figure S9.** (top) Total deaths associated to PM<sub>2.5</sub> (left) per 10×10 km<sup>2</sup> area and (right) summed up for each country, using the Integrated Exposure-Response (IER) method (Burnett et al., 2014). These values are derived from satellite. (bottom) Same as above, but using the Global Exposure Mortality Model (GEMM) (Burnett et al., 2018) for PM<sub>2.5</sub> per 10×10 km<sup>2</sup> area (left) and summed up for each country (right). Premature mortality was determined with PM<sub>2.5</sub> derived by the methods described in van Donkelaar (2015), which includes satellite and ground-based observations of aerosol.



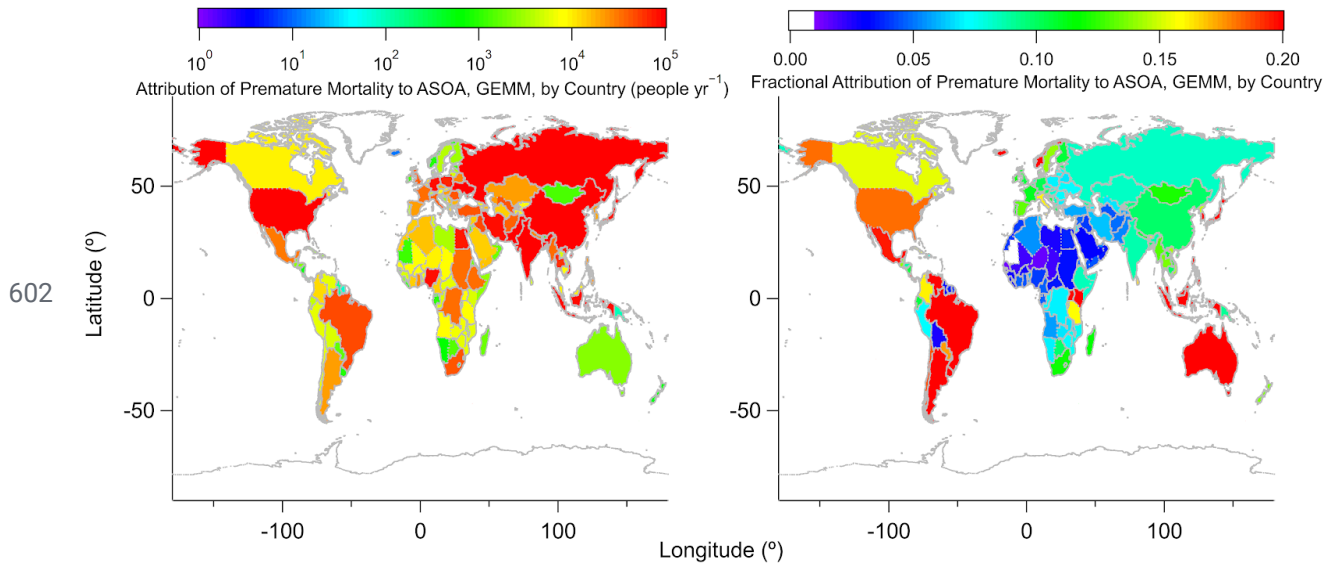
592 **Figure S10.** Same as Fig. 8, where top are the results per 10×10 km<sup>2</sup> area for the attribution of  
 593 premature mortality to ASOA (people yr<sup>-1</sup>, left) and fractional attribution of premature mortality  
 594 to ASOA for one year (right) by the IER method. See Fig. 8 for per country comparison.



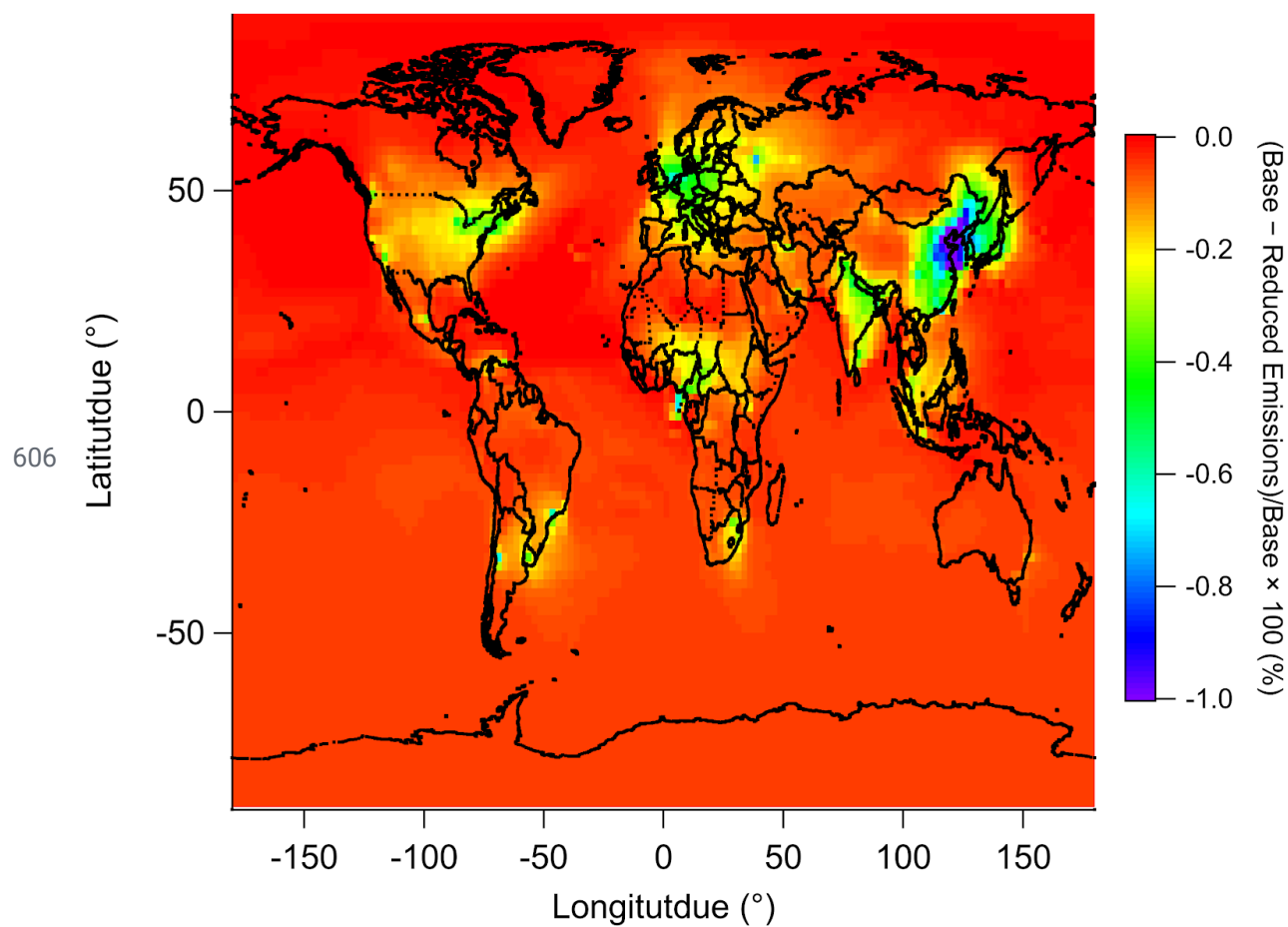
**Figure S11.** Comparison of satellite retrieved PM<sub>2.5</sub> (upper left) versus modeled PM<sub>2.5</sub> (upper right). (Bottom) Fractional contribution of ASOA to total modeled PM<sub>2.5</sub>.

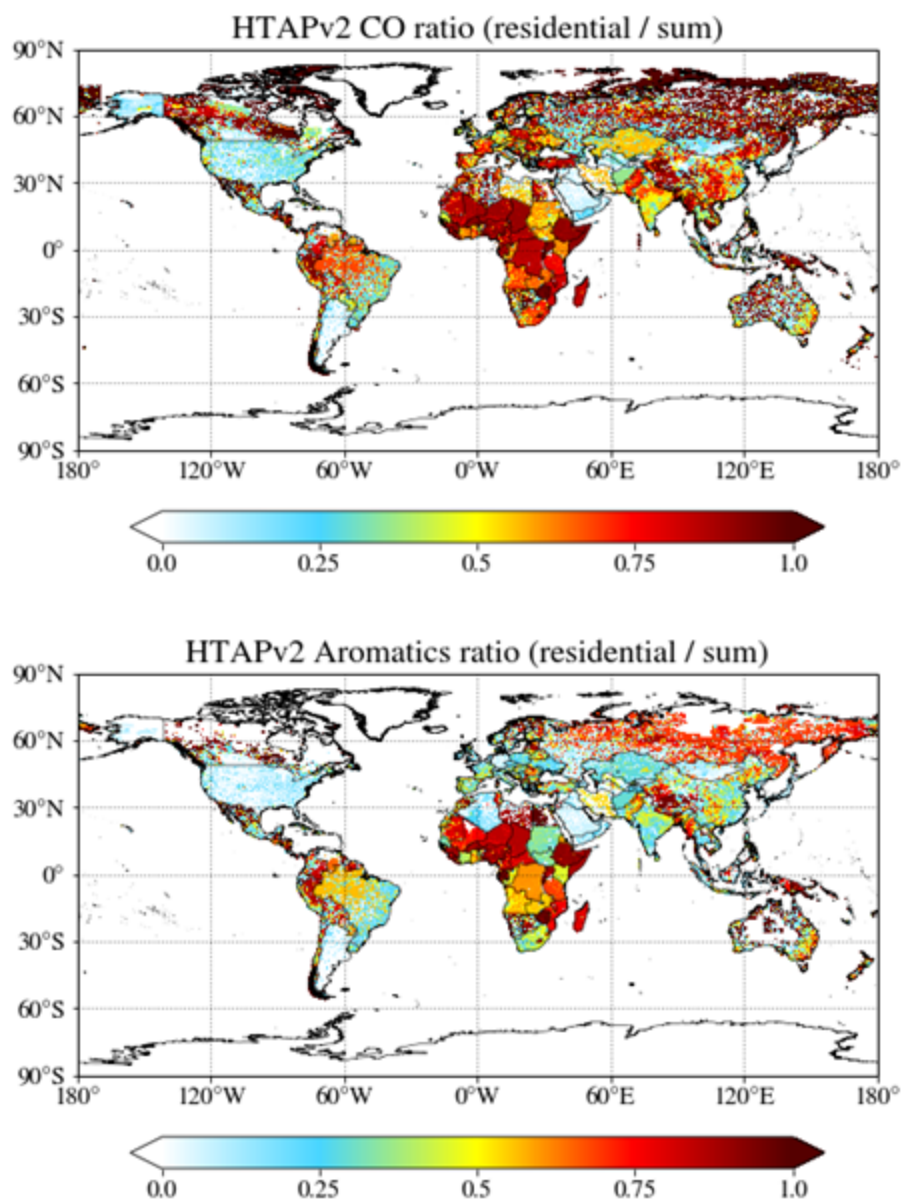


**Figure S12.** Same as Fig. S10, but using the GEMM from Burnett et al. (2018). (top). (Left) Attribution of premature mortality to ASOA per 10×10 km<sup>2</sup> area (people yr<sup>-1</sup>) and (Right) fractional attribution of premature mortality to ASOA per 10×10<sup>2</sup> km for one year.



**Figure S13.** Same as Fig. S12 but summed up for each country for the (left) attribution of premature mortality to ASOA (people yr<sup>-1</sup>) and (right) the fractional attribution of premature mortality to ASOA for one year.





608

609 **Figure S15.** (top) Fractional contribution of CO emissions from residential sources to total  
 610 emission sources from HTaP. (bottom) Fractional contribution of BTEX emissions from  
 611 residential sources to total emission sources from HTAP. Residential sources include small-scale  
 612 combustion, such as heating and cooking, which may include solid-fuel emissions.



## 613 References

- 614 Apel, E. C., Emmons, L. K., Karl, T., Flocke, F., Hills, a. J., Madronich, S., Lee-Taylor, J., Fried,  
615 A., Weibring, P., Walega, J., Richter, D., Tie, X., Mauldin, L., Campos, T., Weinheimer, A.,  
616 Knapp, D., Sive, B., Kleinman, L., Springston, S., Zaveri, R., Ortega, J., Voss, P., Blake, D.,  
617 Baker, A., Warneke, C., Welsh-Bon, D., de Gouw, J., Zheng, J., Zhang, R., Rudolph, J.,  
618 Junkermann, W. and Riemer, D. D.: Chemical evolution of volatile organic compounds in the  
619 outflow of the Mexico City Metropolitan area, *Atmos. Chem. Phys.*, 10(5), 2353–2375, 2010.
- 620 Atkinson, R. and Arey, J.: Atmospheric Degradation of Volatile Organic Compounds, *Chem.*  
621 *Rev.*, 103, 4605–4638, 2003.
- 622 Atkinson, R., Baulch, D. L., Cox, R. A., Crowley, J. N., Hampson, R. F., Hynes, R. G., Jenkin,  
623 M. E., Rossi, M. J., Troe, J. and IUPAC Subcommittee: Evaluated kinetic and photochemical  
624 data for atmospheric chemistry: Volume II - gas phase reactions of organic species, *Atmos.*  
625 *Chem. Phys.*, 6(11), 3625–4055, 2006.
- 626 Bahreini, R., Ervens, B., Middlebrook, A. M., Warneke, C., de Gouw, J. A., DeCarlo, P. F.,  
627 Jimenez, J. L., Brock, C. A., Neuman, J. A., Ryerson, T. B., Stark, H., Atlas, E., Brioude, J.,  
628 Fried, A., Holloway, J. S., Peischl, J., Richter, D., Walega, J., Weibring, P., Wollny, A. G. and  
629 Fehsenfeld, F. C.: Organic aerosol formation in urban and industrial plumes near Houston and  
630 Dallas, Texas, *J. Geophys. Res.*, 114, 1185, 2009.
- 631 Baker, A. K., Beyersdorf, A. J., Doezeema, L. A., Katzenstein, A., Meinardi, S., Simpson, I. J.,  
632 Blake, D. R. and Sherwood Rowland, F.: Measurements of nonmethane hydrocarbons in 28  
633 United States cities, *Atmos. Environ.*, 42(1), 170–182, 2008.
- 634 Bey, I., Jacob, D. J., Yantosca, R. M., Logan, J. A., Field, B. D., Fiore, A. M., Li, Q., Liu, H. Y.,  
635 Mickley, L. J. and Schultz, M. G.: Global modeling of tropospheric chemistry with assimilated  
636 meteorology: Model description and evaluation, *J. Geophys. Res. D: Atmos.*, 106(D19),  
637 23073–23095, 2001.
- 638 Blake, N. J., Blake, D. R., Simpson, I. J., Meinardi, S., Swanson, A. L., Lopez, J. P., Katzenstein,  
639 A. S., Barletta, B., Shirai, T., Atlas, E., Sachse, G., Avery, M., Vay, S., Fuelberg, H. E., Kiley, C.  
640 M., Kita, K. and Rowland, F. S.: NMHCs and halocarbons in Asian continental outflow during  
641 the Transport and Chemical Evolution over the Pacific (TRACE-P) Field Campaign: Comparison  
642 with PEM-West B, *Journal of Geophysical Research-Atmospheres*, 108(D20), 8806, 2003.
- 643 Bohn, B. and Zetzsch, C.: Kinetics and mechanism of the reaction of OH with the  
644 trimethylbenzenes – experimental evidence for the formation of adduct isomers, *Phys. Chem.*  
645 *Chem. Phys.*, 14(40), 13933, 2012.
- 646 Bon, D. M., Ulbrich, I. M., de Gouw, J. A., Warneke, C., Kuster, W. C., Alexander, M. L., Baker,  
647 A., Beyersdorf, A. J., Blake, D., Fall, R., Jimenez, J. L., Herndon, S. C., Huey, L. G., Knighton,  
648 W. B., Ortega, J., Springston, S. and Vargas, O.: Measurements of volatile organic compounds at  
649 a suburban ground site (T1) in Mexico City during the MILAGRO 2006 campaign: measurement

650 comparison, emission ratios, and source attribution, *Atmos. Chem. Phys.*, 11(6), 2399–2421,  
651 2011.

652 Burnett, R., Chen, H., Szyszkowicz, M., Fann, N., Hubbell, B., Pope, C. A., Apte, J. S., Brauer,  
653 M., Cohen, A., Weichenthal, S., Coggins, J., Di, Q., Brunekreef, B., Frostad, J., Lim, S. S., Kan,  
654 H., Walker, K. D., Thurston, G. D., Hayes, R. B., Lim, C. C., Turner, M. C., Jerrett, M., Krewski,  
655 D., Gapstur, S. M., Diver, W. R., Ostro, B., Goldberg, D., Crouse, D. L., Martin, R. V., Peters, P.,  
656 Pinault, L., Tjepkema, M., van Donkelaar, A., Villeneuve, P. J., Miller, A. B., Yin, P., Zhou, M.,  
657 Wang, L., Janssen, N. A. H., Marra, M., Atkinson, R. W., Tsang, H., Quoc Thach, T., Cannon, J.  
658 B., Allen, R. T., Hart, J. E., Laden, F., Cesaroni, G., Forastiere, F., Weinmayr, G., Jaensch, A.,  
659 Nagel, G., Concin, H. and Spadaro, J. V.: Global estimates of mortality associated with long-term  
660 exposure to outdoor fine particulate matter, *Proc. Natl. Acad. Sci. U. S. A.*, 115(38), 9592–9597,  
661 2018.

662 Burnett, R. T., Pope, C. A., Ezzati, M., Olives, C., Lim, S. S., Mehta, S., Shin, H. H., Singh, G.,  
663 Hubbell, B., Brauer, M., Anderson, H. R., Smith, K. R., Balmes, J. R., Bruce, N. G., Kan, H.,  
664 Laden, F., Prüss-Ustün, A., Turner, M. C., Gapstur, S. M., Diver, W. R. and Cohen, A.: An  
665 integrated risk function for estimating the global burden of disease attributable to ambient fine  
666 particulate matter exposure, *Environ. Health Perspect.*, 122(4), 397–403, 2014.

667 CARB: CEPAM: 2013 Almanac - Standard Emissions Tool, [online] Available from:  
668 <https://www.arb.ca.gov/app/emsmv/fcemssumcat2013.php>, 2013.

669 Cárdenas, L. M., Brassington, D. J., Allan, B. J., Coe, H., Alicke, B., Platt, U., Wilson, K. M.,  
670 Plane, J. M. C. and Penkett, S. A.: Intercomparison of Formaldehyde Measurements in Clean and  
671 Polluted Atmospheres, *J. Atmos. Chem.*, 37(1), 53–80, 2000.

672 Cazorla, M., Wolfe, G. M., Bailey, S. A., Swanson, A. K., Arkinson, H. L. and Hanisco, T. F.: A  
673 new airborne laser-induced fluorescence instrument for in situ detection of formaldehyde  
674 throughout the troposphere and lower stratosphere, *Atmos. Meas. Tech.*, 8(2), 541–552, 2015.

675 CCPR: The California Consumer Products Regulation., 2015.

676 Davis, M. S.: 2005 Architectural Coatings Survey Final Report, CARB., 2007.

677 DeCarlo, P. F., Kimmel, J. R., Trimborn, A., Northway, M. J., Jayne, J. T., Aiken, A. C., Gonin,  
678 M., Fuhrer, K., Horvath, T., Docherty, K. S., Worsnop, D. R. and Jimenez, J. L.:  
679 Field-deployable, high-resolution, time-of-flight aerosol mass spectrometer, *Anal. Chem.*,  
680 78(24), 8281–8289, 2006.

681 DeCarlo, P. F., Ulbrich, I. M., Crounse, J., de Foy, B., Dunlea, E. J., Aiken, A. C., Knapp, D.,  
682 Weinheimer, A. J., Campos, T., Wennberg, P. O. and Jimenez, J. L.: Investigation of the sources  
683 and processing of organic aerosol over the Central Mexican Plateau from aircraft measurements  
684 during MILAGRO, *Atmos. Chem. Phys.*, 10(12), 5257–5280, 2010.

685 van Donkelaar, A., Martin, R. V., Brauer, M. and Boys, B. L.: Use of Satellite Observations for  
686 Long-Term Exposure Assessment of Global Concentrations of Fine Particulate Matter, *Environ.*

687 Health Perspect., 123(2), 135–143, 2015.

688 Drewnick, F., Hings, S. S., DeCarlo, P., Jayne, J. T., Gonin, M., Fuhrer, K., Weimer, S., Jimenez,  
689 J. L., Demerjian, K. L., Borrmann, S. and Worsnop, D. R.: A New Time-of-Flight Aerosol Mass  
690 Spectrometer (TOF-AMS)—Instrument Description and First Field Deployment, *Aerosol Sci.*  
691 *Technol.*, 39(7), 637–658, 2005.

692 Duncan Fairlie, T., Jacob, D. J. and Park, R. J.: The impact of transpacific transport of mineral  
693 dust in the United States, *Atmos. Environ.*, 41(6), 1251–1266, 2007.

694 Dunmore, R. E., Hopkins, J. R., Lidster, R. T., Lee, J. D., Evans, M. J., Rickard, A. R., Lewis, A.  
695 C. and Hamilton, J. F.: Diesel-related hydrocarbons can dominate gas phase reactive carbon in  
696 megacities, *Atmos. Chem. Phys.*, 15, 9983–9996, 2015.

697 Dzepina, K., Volkamer, R. M., Madronich, S., Tulet, P., Ulbrich, I. M., Zhang, Q., Cappa, C. D.,  
698 Ziemann, P. J. and Jimenez, J. L.: Evaluation of recently-proposed secondary organic aerosol  
699 models for a case study in Mexico City, *Atmos. Chem. Phys.*, 9(15), 5681–5709, 2009.

700 EMEP/EEA: EMEP/EEA Air Pollutant Emission Inventory Guidebook 2016, EEA,  
701 Luxembourg., 2016.

702 EPA: SPECIATE v4.4, US Environmental Protection Agency., 2014.

703 Fisher, J. A., Jacob, D. J., Travis, K. R., Kim, P. S., Marais, E. A., Miller, C. C., Yu, K., Zhu, L.,  
704 Yantosca, R. M., Sulprizio, M. P., Mao, J., Wennberg, P. O., Crounse, J. D., Teng, A. P., Nguyen,  
705 T. B., Clair, J. M. S., Cohen, R. C., Romer, P., Nault, B. A., Wooldridge, P. J., Jimenez, J. L.,  
706 Campuzano-Jost, P., Day, D. A., Hu, W., Shepson, P. B., Xiong, F., Blake, D. R., Goldstein, A.  
707 H., Misztal, P. K., Hanisco, T. F., Wolfe, G. M., Ryerson, T. B., Wisthaler, A. and Mikoviny, T.:  
708 Organic nitrate chemistry and its implications for nitrogen budgets in an isoprene- and  
709 monoterpene-rich atmosphere: Constraints from aircraft (SEAC<sup>4</sup>RS) and ground-based (SOAS)  
710 observations in the Southeast US, *Atmos. Chem. Phys.*, 16(9), doi:10.5194/acp-16-5969-2016,  
711 2016.

712 Fried, A., Crawford, J., Olson, J., Walega, J., Potter, W., Wert, B., Jordan, C., Anderson, B.,  
713 Shetter, R., Lefer, B., Blake, D., Blake, N., Meinardi, S., Heikes, B., O’Sullivan, D., Snow, J.,  
714 Fuelberg, H., Kiley, C. M., Sandholm, S., Tan, D., Sachse, G., Singh, H., Faloona, I., Harward,  
715 C. N. and Carmichael, G. R.: Airborne tunable diode laser measurements of formaldehyde during  
716 TRACE-P: Distributions and box model comparisons, *J. Geophys. Res. D: Atmos.*, 108(D20),  
717 8798, 2003.

718 Gately, C. K., Hutrya, L. R. and Wing, I. S.: Cities, traffic, and CO<sub>2</sub>: A multidecadal assessment  
719 of trends, drivers, and scaling relationships, *Proc. Natl. Acad. Sci. U. S. A.*, 112(16), 4999–5004,  
720 2015.

721 Gentner, D. R., Isaacman, G., Worton, D. R., Chan, A. W. H., Dallmann, T. R., Davis, L., Liu, S.,  
722 Day, D. A., Russell, L. M., Wilson, K. R., Weber, R., Guha, A., Harley, R. A. and Goldstein, A.  
723 H.: Elucidating secondary organic aerosol from diesel and gasoline vehicles through detailed

724 characterization of organic carbon emissions, *Proc. Natl. Acad. Sci. U. S. A.*, 109(45),  
725 18318–18323, 2012.

726 Gentner, D. R., Worton, D. R., Isaacman, G., Davis, L. C., Dallmann, T. R., Wood, E. C.,  
727 Herndon, S. C., Goldstein, A. H. and Harley, R. A.: Chemical Composition of Gas-Phase  
728 Organic Carbon Emissions from Motor Vehicles and Implications for Ozone Production,  
729 *Environ. Sci. Technol.*, 47(20), 11837–11848, 2013.

730 Gerbig, C., Schmitgen, S., Kley, D., Volz-Thomas, A., Dewey, K. and Haaks, D.: An improved  
731 fast-response vacuum-UV resonance fluorescence CO instrument, *J. Geophys. Res. D: Atmos.*,  
732 104(D1), 1699–1704, 1999.

733 Gilman, J. B., Burkhardt, J. F., Lerner, B. M., Williams, E. J., Kuster, W. C., Goldan, P. D.,  
734 Murphy, P. C., Warneke, C., Fowler, C., Montzka, S. A., Miller, B. R., Miller, L., Oltmans, S. J.,  
735 Ryerson, T. B., Cooper, O. R., Stohl, A. and de Gouw, J. A.: Ozone variability and halogen  
736 oxidation within the Arctic and sub-Arctic springtime boundary layer, *Atmos. Chem. Phys.*,  
737 10(21), 10223–10236, 2010.

738 de Gouw, J. A., Middlebrook, A. M., Warneke, C., Goldan, P. D., Kuster, W. C., Roberts, J. M.,  
739 Fehsenfeld, F. C., Worsnop, D. R., Canagaratna, M. R., Pszenny, A. A. P., Keene, W. C.,  
740 Marchewka, M., Bertman, S. B. and Bates, T. S.: Budget of organic carbon in a polluted  
741 atmosphere: Results from the New England Air Quality Study in 2002, *J. Geophys. Res. D:*  
742 *Atmos.*, 110(16), 1–22, 2005.

743 de Gouw, J. A., Gilman, J. B., Kim, S.-W., Lerner, B. M., Isaacman-VanWertz, G., McDonald, B.  
744 C., Warneke, C., Kuster, W. C., Lefer, B. L., Griffith, S. M., Dusanter, S., Stevens, P. S. and  
745 Stutz, J.: Chemistry of Volatile Organic Compounds in the Los Angeles basin: Nighttime  
746 Removal of Alkenes and Determination of Emission Ratios, *J. Geophys. Res.: Atmos.*, 122(21),  
747 11,843–11,861, 2017.

748 Griffith, S. M., Hansen, R. F., Dusanter, S., Michoud, V., Gilman, J. B., Kuster, W. C., Veres, P.  
749 R., Graus, M., Gouw, J. A., Roberts, J., Young, C., Washenfelder, R., Brown, S. S., Thalman, R.,  
750 Waxman, E., Volkamer, R., Tsai, C., Stutz, J., Flynn, J. H., Grossberg, N., Lefer, B., Alvarez, S.  
751 L., Rappenglueck, B., Mielke, L. H., Osthoff, H. D. and Stevens, P. S.: Measurements of  
752 hydroxyl and hydroperoxy radicals during CalNex-LA: Model comparisons and radical budgets,  
753 *J. Geophys. Res. D: Atmos.*, 121(8), 4211–4232, 2016.

754 Hassler, B., McDonald, B. C., Frost, G. J., Borbon, A., Carslaw, D. C., Civerolo, K., Granier, C.,  
755 Monks, P. S., Monks, S., Parrish, D. D., Pollack, I. B., Rosenlof, K. H., Ryerson, T. B., von  
756 Schneidemesser, E. and Trainer, M.: Analysis of long-term observations of NO<sub>x</sub> and CO in  
757 megacities and application to constraining emissions inventories, *Geophys. Res. Lett.*, 43(18),  
758 9920–9930, 2016.

759 Hayes, P. L., Ortega, A. M., Cubison, M. J., Froyd, K. D., Zhao, Y., Cliff, S. S., Hu, W. W.,  
760 Toohey, D. W., Flynn, J. H., Lefer, B. L., Grossberg, N., Alvarez, S., Rappenglück, B., Taylor, J.  
761 W., Allan, J. D., Holloway, J. S., Gilman, J. B., Kuster, W. C., de Gouw, J. A., Massoli, P.,

762 Zhang, X., Liu, J., Weber, R. J., Corrigan, A. L., Russell, L. M., Isaacman, G., Worton, D. R.,  
 763 Kreisberg, N. M., Goldstein, A. H., Thalman, R., Waxman, E. M., Volkamer, R., Lin, Y. H.,  
 764 Surratt, J. D., Kleindienst, T. E., Offenberg, J. H., Dusanter, S., Griffith, S., Stevens, P. S.,  
 765 Brioude, J., Angevine, W. M. and Jimenez, J. L.: Organic aerosol composition and sources in  
 766 Pasadena, California, during the 2010 CalNex campaign, *J. Geophys. Res. D: Atmos.*, 118(16),  
 767 9233–9257, 2013.

768 Hayes, P. L., Carlton, A. G., Baker, K. R., Ahmadov, R., Washenfelder, R. A., Alvarez, S.,  
 769 Rappenglück, B., Gilman, J. B., Kuster, W. C., de Gouw, J. A., Zotter, P., Prévôt, A. S. H.,  
 770 Szidat, S., Kleindienst, T. E., Ma, P. K. and Jimenez, J. L.: Modeling the formation and aging of  
 771 secondary organic aerosols in Los Angeles during CalNex 2010, *Atmos. Chem. Phys.*, 15(10),  
 772 5773–5801, 2015.

773 Hodzic, A. and Jimenez, J. L.: Modeling anthropogenically controlled secondary organic  
 774 aerosols in a megacity: A simplified framework for global and climate models, *Geosci. Model*  
 775 *Dev.*, 4(4), 901–917, 2011.

776 Hodzic, A., Jimenez, J. L., Madronich, S., Canagaratna, M. R., DeCarlo, P. F., Kleinman, L. and  
 777 Fast, J.: Modeling organic aerosols in a megacity: potential contribution of semi-volatile and  
 778 intermediate volatility primary organic compounds to secondary organic aerosol formation,  
 779 *Atmos. Chem. Phys.*, 10(12), 5491–5514, 2010.

780 Huey L Tanner D Slusher D Dibb J Arimoto R Chen G Davis D Buhr M Nowak J Mauldin R  
 781 Eisele F, K. E.: CIMS measurements of HNO<sub>3</sub> and SO<sub>2</sub> at the South Pole during ISCAT 2000,  
 782 *Atmos. Environ.*, 38(32), 5411–5421, 2004.

783 Hu, W., Hu, M., Hu, W., Jimenez, J. L., Yuan, B., Chen, W., Wang, M., Wu, Y., Chen, C., Wang,  
 784 Z., Peng, J., Zeng, L. and Shao, M.: Chemical composition, sources, and aging process of  
 785 submicron aerosols in Beijing: Contrast between summer and winter, *J. Geophys. Res. D:*  
 786 *Atmos.*, 121(4), 1955–1977, 2016.

787 IEA: World energy balances, IEA World Energy Statistics and Balances,  
 788 doi:10.1787/data-00521-en, 2019.

789 Jaeglé, L., Quinn, P. K., Bates, T. S., Alexander, B. and Lin, J.-T.: Global distribution of sea salt  
 790 aerosols: new constraints from in situ and remote sensing observations, *Atmos. Chem. Phys.*,  
 791 11(7), 3137–3157, 2011.

792 Janssens-Maenhout, G., Crippa, M., Guizzardi, D., Dentener, F., Muntean, M., Pouliot, G.,  
 793 Keating, T., Zhang, Q., Kurokawa, J., Wankmüller, R., Denier van der Gon, H., Kuenen, J. J. P.,  
 794 Klimont, Z., Frost, G., Darras, S., Koffi, B. and Li, M.: HTAP\_v2.2: a mosaic of regional and  
 795 global emission grid maps for 2008 and 2010 to study hemispheric transport of air pollution,  
 796 *Atmos. Chem. Phys.*, 15(19), 11411–11432, 2015.

797 Jathar, S. H., Gordon, T. D., Hennigan, C. J., Pye, H. O. T., Pouliot, G., Adams, P. J., Donahue,  
 798 N. M. and Robinson, A. L.: Unspeciated organic emissions from combustion sources and their

799 influence on the secondary organic aerosol budget in the United States, *Proc. Natl. Acad. Sci. U.*  
800 *S. A.*, 111(29), 10473–10478, 2014.

801 Jayne, J. T., Leard, D. C., Zhang, X. F., Davidovits, P., Smith, K. A., Kolb, C. E. and Worsnop,  
802 D. R.: Development of an aerosol mass spectrometer for size and composition analysis of  
803 submicron particles, *Aerosol Sci. Technol.*, 33(1-2), 49–70, 2000.

804 Kaiser, J., Jacob, D. J., Zhu, L., Travis, K. R., Fisher, J. A., González Abad, G., Zhang, L.,  
805 Zhang, X., Fried, A., Crounse, J. D., St. Clair, J. M. and Wisthaler, A.: High-resolution inversion  
806 of OMI formaldehyde columns to quantify isoprene emission on ecosystem-relevant scales:  
807 application to the southeast US, *Atmos. Chem. Phys.*, 18(8), 5483–5497, 2018.

808 Kim, S., Huey, L. G., Stickel, R. E., Tanner, D. J., Crawford, J. H., Olson, J. R., Chen, G., Brune,  
809 W. H., Ren, X., Leshner, R., Wooldridge, P. J., Bertram, T. H., Perring, A., Cohen, R. C., Lefer, B.  
810 L., Shetter, R. E., Avery, M., Diskin, G. and Sokolik, I.: Measurement of HO<sub>2</sub>NO<sub>2</sub> in the free  
811 troposphere during the Intercontinental Chemical Transport Experiment–North America 2004, *J.*  
812 *Geophys. Res. D: Atmos.*, 112, D12S01, 2007.

813 Kleinman, L. I., Daum, P. H., Lee, Y.-N., Senum, G. I., Springston, S. R., Wang, J., Berkowitz,  
814 C., Hubbe, J., Zaveri, R. A., Brechtel, F. J., Jayne, J., Onasch, T. B. and Worsnop, D.: Aircraft  
815 observations of aerosol composition and ageing in New England and Mid-Atlantic States during  
816 the summer 2002 New England Air Quality Study field campaign, *J. Geophys. Res. D: Atmos.*,  
817 112(D9), D09310, 2007.

818 Koo, B., Knipping, E. and Yarwood, G.: 1.5-Dimensional volatility basis set approach for  
819 modeling organic aerosol in CAMx and CMAQ, *Atmos. Environ.*, 95, 158–164, 2014.

820 Kuwata, M., Zorn, S. R. and Martin, S. T.: Using Elemental Ratios to Predict the Density of  
821 Organic Material Composed of Carbon, Hydrogen, and Oxygen, *Environ. Sci. Technol.*, 46(2),  
822 787–794, 2012.

823 Langford, B., Nemitz, E., House, E., Phillips, G. J., Famulari, D., Davison, B., Hopkins, J. R.,  
824 Lewis, A. C. and Hewitt, C. N.: Fluxes and concentrations of volatile organic compounds above  
825 central London, UK, *Atmos. Chem. Phys.*, 10(2), 627–645, 2010.

826 Li, M., Zhang, Q., Streets, D. G., He, K. B., Cheng, Y. F., Emmons, L. K., Huo, H., Kang, S. C.,  
827 Lu, Z., Shao, M., Su, H., Yu, X. and Zhang, Y.: Mapping Asian anthropogenic emissions of  
828 non-methane volatile organic compounds to multiple chemical mechanisms, *Atmos. Chem.*  
829 *Phys.*, 14(11), 5617–5638, 2014.

830 Li, M., Liu, H., Geng, G., Hong, C., Liu, F., Song, Y., Tong, D., Zheng, B., Cui, H., Man, H.,  
831 Zhang, Q. and He, K.: Anthropogenic emission inventories in China: a review, *Natl Sci Rev*,  
832 4(6), 834–866, 2017.

833 Li, M., Zhang, Q., Zheng, B., Tong, D., Lei, Y., Liu, F., Chaopeng, H., Kang, S., Yan, L., Zhang,  
834 Y., Bo, Y., Su, H., Cheng, Y. and He, K.: Persistent growth of anthropogenic non-methane  
835 volatile organic compound (NMVOC) emissions in China during 1990-2017: drivers, speciation



836 and ozone formation potential, *Atmos. Chem. Phys.*, 19, 8897–8913, 2019.

837 Liu, F., Zhang, Q., Tong, D., Zheng, B., Li, M., Huo, H. and He, K. B.: High-resolution  
838 inventory of technologies, activities, and emissions of coal-fired power plants in China from  
839 1990 to 2010, *Atmos. Chem. Phys.*, 15(23), 13299–13317, 2015.

840 Lu, Q., Zhao, Y. and Robinson, A. L.: Comprehensive organic emission profiles for gasoline,  
841 diesel, and gas-turbine engines including intermediate and semi-volatile organic compound  
842 emissions, *Atmos. Chem. Phys.*, 18, 17637–17654, 2018.

843 Ma, P. K., Zhao, Y., Robinson, A. L., Worton, D. R., Goldstein, A. H., Ortega, A. M., Jimenez, J.  
844 L., Zotter, P., Prévôt, A. S. H., Szidat, S. and Hayes, P. L.: Evaluating the impact of new  
845 observational constraints on P-S/IVOC emissions, multi-generation oxidation, and chamber wall  
846 losses on SOA modeling for Los Angeles, CA, *Atmos. Chem. Phys.*, 17(15), 9237–9259, 2017.

847 Marais, E. A., Jacob, D. J., Jimenez, J. L., Campuzano-Jost, P., Day, D. A., Hu, W., Krechmer, J.,  
848 Zhu, L., Kim, P. S., Miller, C. C., Fisher, J. A., Travis, K., Yu, K., Hanisco, T. F., Wolfe, G. M.,  
849 Arkinson, H. L., Pye, H. O. T., Froyd, K. D., Liao, J. and McNeill, V. F.: Aqueous-phase  
850 mechanism for secondary organic aerosol formation from isoprene: application to the southeast  
851 United States and co-benefit of SO<sub>2</sub> emission controls, *Atmos. Chem. Phys.*, 16(3), 1603–1618,  
852 2016.

853 Matheson, R. R.: 20th- to 21st-Century Technological Challenges in Soft Coatings, *Science*,  
854 297(5583), 976–979, 2002.

855 McDonald, B. C., Gentner, D. R., Goldstein, A. H. and Harley, R. A.: Long-Term Trends in  
856 Motor Vehicle Emissions in U.S. Urban Areas, *Environ. Sci. Technol.*, 47(17), 10022–10031,  
857 2013.

858 McDonald, B. C., Goldstein, A. H. and Harley, R. A.: Long-Term Trends in California Mobile  
859 Source Emissions and Ambient Concentrations of Black Carbon and Organic Aerosol, *Environ.*  
860 *Sci. Technol.*, 49(8), 5178–5188, 2015.

861 McDonald, B. C., de Gouw, J. A., Gilman, J. B., Jathar, S. H., Akherati, A., Cappa, C. D.,  
862 Jimenez, J. L., Lee-Taylor, J., Hayes, P. L., McKeen, S. A., Cui, Y. Y., Kim, S.-W., Gentner, D.  
863 R., Isaacman-VanWertz, G., Goldstein, A. H., Harley, R. A., Frost, G. J., Roberts, J. M., Ryerson,  
864 T. B. and Trainer, M.: Volatile chemical products emerging as largest petrochemical source of  
865 urban organic emissions, *Science*, 359(6377), 760–764, 2018.

866 Mollner, A. K., Valluvadasan, S., Feng, L., Sprague, M. K., Okumura, M., Milligan, D. B., Bloss,  
867 W. J., Sander, S. P., Martien, P. T., Harley, R. A., McCoy, A. B. and Carter, W. P. L.: Rate of Gas  
868 Phase Association of Hydroxyl Radical and Nitrogen Dioxide, *Science*, 330(6004), 646–649,  
869 2010.

870 MOVES: MOVES2014a User Guide., 2015.

871 Nault, B. A., Campuzano-Jost, P., Day, D. A., Schroder, J. C., Anderson, B., Beyersdorf, A. J.,

872 Blake, D. R., Brune, W. H., Choi, Y., Corr, C. A., de Gouw, J. A., Dibb, J., DiGangi, J. P., Diskin,  
 873 G. S., Fried, A., Huey, L. G., Kim, M. J., Knote, C. J., Lamb, K. D., Lee, T., Park, T., Pusede, S.  
 874 E., Scheuer, E., Thornhill, K. L., Woo, J.-H. and Jimenez, J. L.: Secondary Organic Aerosol  
 875 Production from Local Emissions Dominates the Organic Aerosol Budget over Seoul, South  
 876 Korea, during KORUS-AQ, *Atmos. Chem. Phys.*, 18, 17769–17800, 2018.

877 NEI: National Emissions Inventory (NEI) 2011, version 1, Research Triangle Park., 2015.

878 Pai, S. J., Heald, C. L., Pierce, J. R., Farina, S. C., Marais, E. A., Jimenez, J. L.,  
 879 Campuzano-Jost, P., Nault, B. A., Middlebrook, A. M., Coe, H., Shilling, J. E., Bahreini, R.,  
 880 Dingle, J. H. and Vu, K.: An evaluation of global organic aerosol schemes using airborne  
 881 observations, *Atmos. Chem. Phys.*, 20(5), 2637–2665, 2020.

882 Pankow, J. F. and Asher, W. E.: SIMPOL.1: a simple group contribution method for predicting  
 883 vapor pressures and enthalpies of vaporization of multifunctional organic compounds, *Atmos.*  
 884 *Chem. Phys.*, 8(10), 2773–2796, 2008.

885 Park, R. J., Jacob, D. J., Palmer, P. I., Clarke, A. D., Weber, R. J., Zondlo, M. A., Eisele, F. L.,  
 886 Bandy, A. R., Thornton, D. C., Sachse, G. W. and Bond, T. C.: Export efficiency of black carbon  
 887 aerosol in continental outflow: Global implications, *J. Geophys. Res. D: Atmos.*, 110(D11),  
 888 D11205, 2005.

889 Park, R. J., Jacob, D. J., Kumar, N. and Yantosca, R. M.: Regional visibility statistics in the  
 890 United States: Natural and transboundary pollution influences, and implications for the Regional  
 891 Haze Rule, *Atmos. Environ.*, 40(28), 5405–5423, 2006.

892 Peng, Z. and Jimenez, J. L.: KinSim: A Research-Grade, User-Friendly, Visual Kinetics  
 893 Simulator for Chemical-Kinetics and Environmental-Chemistry Teaching, *J. Chem. Educ.*, 96(4),  
 894 806–811, 2019.

895 Pierson, W. R., Schorran, D. E., Fujita, E. M., Sagebiel, J. C., Lawson, D. R. and Tanner, R. L.:  
 896 Assessment of Nontailpipe Hydrocarbon Emissions from Motor Vehicles, *J. Air Waste Manage.*  
 897 *Assoc.*, 49(5), 498–519, 1999.

898 Pollack, I. B., Lerner, B. M. and Ryerson, T. B.: Evaluation of ultraviolet light-emitting diodes  
 899 for detection of atmospheric NO<sub>2</sub> by photolysis - chemiluminescence, *J. Atmos. Chem.*, 65(2-3),  
 900 111–125, 2010.

901 Pye, H. O. T. and Seinfeld, J. H.: A global perspective on aerosol from low-volatility organic  
 902 compounds, *Atmos. Chem. Phys.*, 10, 4377–4401, 2010.

903 Roberts, J. M., Stroud, C. A., Jobson, B. T., Trainer, M., Hereid, D., Williams, E., Fehsenfeld, F.,  
 904 Brune, W., Martinez, M. and Harder, H.: Application of a sequential reaction model to PANs and  
 905 aldehyde measurements in two urban areas, *Geophys. Res. Lett.*, 28(24), 4583–4586, 2001.

906 Roberts, J. M., Flocke, F., Stroud, C. A., Hereid, D., Williams, E., Fehsenfeld, F., Brune, W.,  
 907 Martinez, M. and Harder, H.: Ground-based measurements of peroxydicarboxylic nitric anhydrides



908 (PANs) during the 1999 Southern Oxidants Study Nashville Intensive, *J. Geophys. Res. D:*  
 909 *Atmos.*, 107(D21), 4554, 2002.

910 Robinson, A. L., Donahue, N. M., Shrivastava, M. K., Weitkamp, E. A., Sage, A. M., Grieshop,  
 911 A. P., Lane, T. E., Pierce, J. R. and Pandis, S. N.: Rethinking Organic Aerosols: Semivolatile  
 912 Emissions and Photochemical Aging, *Science*, 315(5816), 1259–1262, 2007.

913 Rubin, J. I., Kean, A. J., Harley, R. A., Millet, D. B. and Goldstein, A. H.: Temperature  
 914 dependence of volatile organic compound evaporative emissions from motor vehicles, *J.*  
 915 *Geophys. Res. D: Atmos.*, 111(D3), D03305, 2006.

916 Rumble, J. R., Ed.: *CRC Handbook of Chemistry and Physics*, 100th Edition, 2019 - 2020,  
 917 Taylor & Francis Group., 2019.

918 Ryerson, T. B., Huey, L. G., Knapp, K., Neuman, J. A., Parrish, D. D., Sueper, D. T. and  
 919 Fehsenfeld, F. C.: Design and initial characterization of an inlet for gas-phase NO<sub>y</sub> measurements  
 920 from aircraft, *J. Geophys. Res. D: Atmos.*, 104(D5), 5483–5492, 1999.

921 Ryerson, T. B., Andrews, A. E., Angevine, W. M., Bates, T. S., Brock, C. A., Cairns, B., Cohen,  
 922 R. C., Cooper, O. R., de Gouw, J. A., Fehsenfeld, F. C., Ferrare, R. A., Fischer, M. L., Flagan, R.  
 923 C., Goldstein, A. H., Hair, J. W., Hardesty, R. M., Hostetler, C. A., Jimenez, J. L., Langford, A.  
 924 O., McCauley, E., McKeen, S. A., Molina, L. T., Nenes, A., Oltmans, S. J., Parrish, D. D.,  
 925 Pederson, J. R., Pierce, R. B., Prather, K., Quinn, P. K., Seinfeld, J. H., Senff, C. J., Sorooshian,  
 926 A., Stutz, J., Surratt, J. D., Trainer, M., Volkamer, R., Williams, E. J. and Wofsy, S. C.: The 2010  
 927 California Research at the Nexus of Air Quality and Climate Change (CalNex) field study, *J.*  
 928 *Geophys. Res. D: Atmos.*, 118(11), 5830–5866, 2013.

929 Sachse, G. W., Hill, G. F., Wade, L. O. and Perry, M. G.: Fast-Response, High-Precision Carbon  
 930 Monoxide Sensor using a Tunable Diode Laser Absorption Technique, *J. Geophys. Res.: Atmos.*,  
 931 92(D2), 2071–2081, 1987.

932 Schroder, J. C., Campuzano-Jost, P., Day, D. A., Shah, V., Larson, K., Sommers, J. M., Sullivan,  
 933 A. P., Campos, T., Reeves, J. M., Hills, A., Hornbrook, R. S., Blake, N. J., Scheuer, E., Guo, H.,  
 934 Fibiger, D. L., McDuffie, E. E., Hayes, P. L., Weber, R. J., Dibb, J. E., Apel, E. C., Jaeglé, L.,  
 935 Brown, S. S., Thronton, J. A. and Jimenez, J. L.: Sources and Secondary Production of Organic  
 936 Aerosols in the Northeastern US during WINTER, *J. Geophys. Res. D: Atmos.*,  
 937 doi:10.1029/2018JD028475, 2018.

938 Seinfeld, J. H. and Pandis, S. N.: *Atmospheric Chemistry and Physics: From Air Pollution to*  
 939 *Climate Change*, Second., John Wiley & Sons, Inc., Hoboken, NJ USA., 2006.

940 Simon, H., Beck, L., Bhave, P. V., Divita, F., Hsu, Y., Luecken, D., Mobley, J. D., Pouliot, G. A.,  
 941 Reff, A., Sarwar, G. and Strum, M.: The development and uses of EPA's SPECIATE database,  
 942 *Atmos. Pollut. Res.*, 1(4), 196–206, 2010.

943 Slusher, D. L., Huey, L. G., Tanner, D. J., Flocke, F. M. and Roberts, J. M.: A thermal  
 944 dissociation-chemical ionization mass spectrometry (TD-CIMS) technique for the simultaneous

945 measurement of peroxyacyl nitrates and dinitrogen pentoxide, *J. Geophys. Res.: Atmos.*,  
946 109(D19), D19315–D19315, 2004.

947 Stutz, J. and Platt, U.: Numerical analysis and estimation of the statistical error of differential  
948 optical absorption spectroscopy measurements with least-squares methods, *Appl. Opt.*, 35(30),  
949 6041, 1996.

950 Stutz, J. and Platt, U.: Improving long-path differential optical absorption spectroscopy with a  
951 quartz-fiber mode mixer, *Appl. Opt.*, 36(6), 1105, 1997.

952 The International GEOS-Chem User Community: geoschem/geos-chem: GEOS-Chem 12.0.0  
953 release, , doi:10.5281/ZENODO.1343547, 2018.

954 Travis, K. R., Jacob, D. J., Fisher, J. A., Kim, P. S., Marais, E. A., Zhu, L., Yu, K., Miller, C. C.,  
955 Yantosca, R. M., Sulprizio, M. P., Thompson, A. M., Wennberg, P. O., Crounse, J. D., St. Clair, J.  
956 M., Cohen, R. C., Laughner, J. L., Dibb, J. E., Hall, S. R., Ullmann, K., Wolfe, G. M., Pollack, I.  
957 B., Peischl, J., Neuman, J. A. and Zhou, X.: Why do models overestimate surface ozone in the  
958 Southeast United States?, *Atmos. Chem. Phys.*, 16(21), 13561–13577, 2016.

959 Tsimpidi, A. P., Karydis, V. A., Zavala, M., Lei, W., Molina, L., Ulbrich, I. M., Jimenez, J. L. and  
960 Pandis, S. N.: Evaluation of the volatility basis-set approach for the simulation of organic aerosol  
961 formation in the Mexico City metropolitan area, *Atmos. Chem. Phys.*, 10(2), 525–546, 2010.

962 Vaden, T. D., Imre, D., Beránek, J., Shrivastava, M. and Zelenyuk, A.: Evaporation kinetics and  
963 phase of laboratory and ambient secondary organic aerosol, *Proc. Natl. Acad. Sci. U. S. A.*,  
964 108(6), 2190–2195, 2011.

965 Vaughan, A. R., Lee, J. D., Shaw, M. D., Misztal, P. K., Metzger, S., Vieno, M., Davison, B.,  
966 Karl, T. G., Carpenter, L. J., Lewis, A. C., Purvis, R. M., Goldstein, A. H. and Hewitt, C. N.:  
967 VOC emission rates over London and South East England obtained by airborne eddy covariance,  
968 *Faraday Discuss.*, 200(0), 599–620, 2017.

969 Wang, M., Shao, M., Chen, W., Yuan, B., Lu, S., Zhang, Q., Zeng, L. and Wang, Q.: A  
970 temporally and spatially resolved validation of emission inventories by measurements of ambient  
971 volatile organic compounds in Beijing, China, *Atmos. Chem. Phys.*, 14(12), 5871–5891, 2014.

972 Warneke, C., McKeen, S. A., de Gouw, J. A., Goldan, P. D., Kuster, W. C., Holloway, J. S.,  
973 Williams, E. J., Lerner, B. M., Parrish, D. D., Trainer, M., Fehsenfeld, F. C., Kato, S., Atlas, E.  
974 L., Baker, A. and Blake, D. R.: Determination of urban volatile organic compound emission  
975 ratios and comparison with an emissions database, *J. Geophys. Res. D: Atmos.*, 112(D10),  
976 doi:10.1029/2006JD007930, 2007.

977 Warneke, C., Veres, P., Holloway, J. S., Stutz, J., Tsai, C., Alvarez, S., Rappenglueck, B.,  
978 Fehsenfeld, F. C., Graus, M., Gilman, J. B. and de Gouw, J. A.: Airborne formaldehyde  
979 measurements using PTR-MS: calibration, humidity dependence, inter-comparison and initial  
980 results, *Atmos. Meas. Tech.*, 4(10), 2345–2358, 2011.

981 Warneke, C., de Gouw, J. A., Holloway, J. S., Peischl, J., Ryerson, T. B., Atlas, E., Blake, D.,  
 982 Trainer, M. and Parrish, D. D.: Multiyear trends in volatile organic compounds in Los Angeles,  
 983 California: Five decades of decreasing emissions, *J. Geophys. Res. D: Atmos.*, 117(D21),  
 984 D00V17, 2012.

985 Weibring, P., Richter, D., Walega, J. G., Rippe, L. and Fried, A.: Difference frequency generation  
 986 spectrometer for simultaneous multispecies detection, *Opt. Express*, 18(26), 27670, 2010.

987 Weinheimer, A. J., Walega, J. G., Ridley, B. A., Gary, B. L., Blake, D. R., Blake, N. J., Rowland,  
 988 F. S., Sachse, G. W., Anderson, B. E. and Collins, J. E.: Meridional distributions of  $\text{NO}_x$ ,  $\text{NO}_y$ ,  
 989 and other species in the lower stratosphere and upper troposphere during AASE II, *Geophys.*  
 990 *Res. Lett.*, 21(23), 2583–2586, 1994.

991 Whalley, L. K., Stone, D., Bandy, B., Dunmore, R., Hamilton, J. F., Hopkins, J., Lee, J. D.,  
 992 Lewis, A. C. and Heard, D. E.: Atmospheric OH reactivity in central London: observations,  
 993 model predictions and estimates of in situ ozone production, *Atmos. Chem. Phys.*, 16(4),  
 994 2109–2122, 2016.

995 Williams, E. J., Roberts, J. M., Baumann, K., Bertman, S. B., Buhr, S., Norton, R. B. and  
 996 Fehsenfeld, F. C.: Variations in  $\text{NO}_y$  composition at Idaho Hill, Colorado, *J. Geophys. Res. D:*  
 997 *Atmos.*, 102(D5), 6297–6314, 1997.

998 Williams, J., Roberts, J. M., Bertman, S. B., Stroud, C. A., Fehsenfeld, F. C., Baumann, K., Buhr,  
 999 M. P., Knapp, K., Murphy, P. C., Nowick, M. and Williams, E. J.: A method for the airborne  
 1000 measurement of PAN, PPN, and MPAN, *J. Geophys. Res. D: Atmos.*, 105(D23), 28943–28960,  
 1001 2000.

1002 Worton, D. R., Isaacman, G., Gentner, D. R., Dallmann, T. R., Chan, A. W. H., Ruehl, C.,  
 1003 Kirchstetter, T. W., Wilson, K. R., Harley, R. A. and Goldstein, A. H.: Lubricating Oil Dominates  
 1004 Primary Organic Aerosol Emissions from Motor Vehicles, *Environ. Sci. Technol.*, 48(7),  
 1005 3698–3706, 2014.

1006 Young, D. E., Allan, J. D., Williams, P. I., Green, D. C., Flynn, M. J., Harrison, R. M., Yin, J.,  
 1007 Gallagher, M. W. and Coe, H.: Investigating the annual behaviour of submicron secondary  
 1008 inorganic and organic aerosols in London, *Atmos. Chem. Phys.*, 15, 6351–6366, 2015.

1009 Yuan, B., Hu, W. W., Shao, M., Wang, M., Chen, W. T., Lu, S. H., Zeng, L. M. and Hu, M.: VOC  
 1010 emissions, evolutions and contributions to SOA formation at a receptor site in eastern China,  
 1011 *Atmos. Chem. Phys.*, 13(17), 8815–8832, 2013.

1012 Zhang, Q., Alfarra, M. R., Worsnop, D. R., James, D., Coe, H., Canagaratna, M. R. and Jimenez,  
 1013 J. L.: Deconvolution and Quantification of Hydrocarbon-like and Oxygenated Organic Aerosols  
 1014 Based on Aerosol Mass Spectrometry Deconvolution and Quantification of Hydrocarbon-like  
 1015 and Oxygenated Organic Aerosols Based on Aerosol Mass Spectrometry, *Environ. Sci. Technol.*,  
 1016 39(13), 4938–4952, 2005.

1017 Zhang, Q., Streets, D. G., Carmichael, G. R., He, K. B., Huo, H., Kannari, A., Klimont, Z., Park,

1018 I. S., Reddy, S., Fu, J. S., Chen, D., Duan, L., Lei, Y., Wang, L. T. and Yao, Z. L.: Asian  
1019 emissions in 2006 for the NASA INTEX-B mission, *Atmos. Chem. Phys.*, 9(14), 5131–5153,  
1020 2009.

1021 Zhao, Y., Hennigan, C. J., May, A. A., Daniel, S., Gouw, J. A. D., Gilman, J. B., Kuster, W. C.  
1022 and Robinson, A. L.: Intermediate-Volatility Organic Compounds: A Large Source of Secondary  
1023 Organic Aerosol, *Environ. Sci. Technol.*, 48(23), 13743–13750, 2014.

1024 Zhao, Y., Saleh, R., Saliba, G., Presto, A. A., Gordon, T. D., Drozd, G. T., Goldstein, A. H.,  
1025 Donahue, N. M. and Robinson, A. L.: Reducing secondary organic aerosol formation from  
1026 gasoline vehicle exhaust, *Proc. Natl. Acad. Sci. U. S. A.*, 114(27), 6984–6989, 2017.

1027 Zheng, B., Huo, H., Zhang, Q., Yao, Z. L., Wang, X. T., Yang, X. F., Liu, H. and He, K. B.:  
1028 High-resolution mapping of vehicle emissions in China in 2008, *Atmos. Chem. Phys.*, 14(18),  
1029 9787–9805, 2014.

1030 Zheng, B., Tong, D., Li, M., Liu, F., Hong, C., Geng, G., Li, H., Li, X., Peng, L., Qi, J., Yan, L.,  
1031 Zhang, Y., Zhao, H., Zheng, Y., He, K. and Zhang, Q.: Trends in China's anthropogenic  
1032 emissions since 2010 as the consequence of clean air actions, *Atmos. Chem. Phys.*, 18(19),  
1033 14095–14111, 2018.

1034